Published in Astronomy and Astrophysics Review 1998, Vol. 8, pp. 237-278.

Centaurus A - NGC 512

F.P. Israel

Sterrewacht Leiden, P.O. Box 9513, 2300 RA Leiden, the Netherlands

Abstract. At a distance of 3.4 Mpc, NGC 5128 (Centaurus A) is by far the nearest active radio galaxy. It is often considered to be the prototype Fanaroff-Riley Class I "low-luminosity" radio galaxy, and as such it plays an important role in our understanding of a major class of active galaxies. Its proximity has spawned numerous detailed investigations of its properties, yielding unrivalled but still incomplete knowledge of its structure and dynamics.

The massive elliptical host galaxy is moderately triaxial and contains a thin, strongly warped disk rich in dust, atomic and molecular gas and luminous young stars. Its globular cluster ensemble has a bimodal distribution of metallicities. Deep optical images reveal faint major axis extensions as well as a system of filaments and shells. These and other characteristics are generally regarded as strong evidence that NGC 5128 has experienced a major merging events at least once in its past.

The galaxy has a very compact, subparsec nucleus exhibiting noticeable intensity variations at radio and X-ray wavelengths, probably powered by accretion events. The central object may be a black hole of moderate mass. Towards the nucleus, rich absorption spectra of atomic hydrogen and various molecular species suggest the presence of significant amounts of material falling into the nucleus, presumably "feeding the monster". Emanating from the nucleus are linear radio/X-ray jets, becoming subrelativistic at a few parsec from the nucleus. At about 5 kpc from the nucleus, the jets expand into plumes. Huge radio lobes extend beyond the plumes out to to 250 kpc. A compact circumnuclear disk with a central cavity surrounds the nucleus. Its plane, although at an angle to the minor axis of the galaxy, is perpendicular to the inner jets. The jet-collimating mechanism, probably connected to the circumnuclear disk, appears to precess on timescales of order a few times 10^7 years.

This review summarizes the present state of knowledge of NGC 5128 and its associated radio source Centaurus A. Underlying physical processes are outside its scope: they are briefly referred to, but not discussed.

Key words: Galaxies: active (11.01.2) - Galaxies: individual: NGC 5128 (11.09.1) - Galaxies: jets (11.10.1) - Infrared: galaxies (13.09.1) - Radio continuum: galaxies (13.18.1) - X-rays: galaxies (13.25.2)

Table of Contents

- INTRODUCTION
  - Historical note
  - Distance
  - Systemic velocity
  - Environment
- THE RADIO SOURCE AND ASSOCIATED FEATURES
  - Overview
  - The outer and middle lobes
  - The inner lobes and outer jet
  - Inner jet structure
  - Optical jet features
- THE GALAXY
  - Overview
  - Globular clusters and metallicity
  - Late-type objects
  - Colours and reddening
- THE DUSTY DISK

- Overview
- Atomic and molecular gas
- Dust emission
- Polarization and extinction

- THE CENTRAL REGION
  - Overview
  - The circumnuclear disk
  - Nuclear emission at infrared wavelengths
  - The radio nucleus and nuclear jet
  - X- and γ-ray emission from the nuclear region
  - Variability of the nucleus

- KINEMATICS AND DYNAMICS
  - Kinematical studies
  - Dynamical models
  - Evolutionary timescale

- THE NUCLEAR ABSORPTION SPECTRUM

- CONCLUDING SUMMARY

- REFERENCES

1. INTRODUCTION

1.1. Historical note

Observing from the Cape of Good Hope, Herschel (1847) was the first to note the peculiar nature of NGC 5128: *"A nebula consisting of two lateral portions and no doubt of a small streak of nebula along the middle of the slit or interval between them, having a star at its extremity"* and *" ... a very problematical object, and must be regarded as forming a genus apart, since it evidently differs from mere `double nebulae' ..."*. Although Hubble (1922) included the galaxy in a list of (mostly galactic) nebulae with line emission, it was mostly ignored until the advent of radio astronomy about 50 years ago (but see Paraskevoulos 1935). Shortly after World War II, Bolton (1948) announced the discovery of six discrete sources of 100 MHz radio emission in addition to the already known case of Cygnus A. Precisely a year later, using their remarkable "cliff-interferometry" technique, Bolton, Stanley & Slee (1949) identified the sources Taurus A, Virgo A and Centaurus A with the nebulous objects M1 (Crab nebula), NGC 4486 (M 87) and NGC 5128 respectively. Although they were actually convinced of the extragalactic nature of the latter two, their published discussion was noncommittal, reflecting referee objections to this notion (R.D. Ekers, private communication). More precise measurements by Mills (1952) confirmed the identification of Centaurus A with NGC 5128. Discussing the nature of optical counterparts to the newly discovered radio sources, Baade & Minkowski (1954) established NGC 5128 as an unusual extragalactic system, located in space well "beyond M 31". They described it as *"... an unresolved E0 nebula with an unusually strong and wide central dark band, a combination highly anomalous for a spherical nebula"* and interpreted it as the interaction or merger of an elliptical and a spiral galaxy. Nevertheless, the merger hypothesis then receded into the background until it was revived some 25 years later by the work of Graham (1979), Dufour et al. (1979), Tubbs (1980) and Malin, Quinn & Graham (1983). It is now the favoured explanation for the unusual characteristics of NGC 5128.

Other radio measurements soon established the nonthermal nature of the radio emission (Haddock, Mayer & Sloanaker 1954). Subsequent radio observations with increased sensitivity yielded ever-larger dimensions for the object until the low-frequency studies by Sheridan (1958) and Shain (1958) first established an overall size of 8° × 4° for Centaurus A - much larger than the 20' size of the optical parent galaxy NGC 5128. A multi-frequency radio study by Cooper, Price & Cole (1965) showed that at decimetre wavelengths the source consists of bright central emission, representing 20% of the total flux density and much larger lower-brightness lobes to the north and south, with 40% of the radio flux each. The advent of interferometric techniques, in particular aperture synthesis radio telescopes with their superior angular resolution, has since led to the discovery of many more similar radio galaxies (*cf.* Allen, Hanbury Brown & Palmer 1963; see review by Miley 1980). It has also become clear that many other elliptical galaxies have more or less pronounced dust lanes (Hawarden et al. 1981; Sadler & Gerhard 1985; van Dokkum & Franx 1995), including the other major southern radio galaxy NGC 1316 (Fornax A).

Both its striking optical appearance (Fig. 1), and its associated giant radio source have made NGC 5128 [(1)] into one of the most extensively studied galaxies in the southern hemisphere. However, in their comprehensive review Ebneter & Balick (1983) point out that NGC 5128 if placed at similar large distances would look very much like other radio elliptical galaxies, in spite of its

apparent peculiarity. By its fortuitous proximity, Centaurus A uniquely allows detailed studies aimed at determining the nature of the galaxy and in particular the origin of the giant radio source it is hosting. A probably incomplete search of the literature published since Ebneter & Balick's (1983) review reveals over a hundred refereed papers mentioning Centaurus A in the title, whereas in the same period the number of papers referring to Centaurus A was almost 700. This review focusses on the observed properties of Centaurus A / NGC 5128 and their immediate interpretation. For a more complete review of the early work up to 1983, the reader is referred to Ebneter & Balick (1983), and for more general information to recent proceedings such as "The Second Stromlo Symposium - The Nature of Elliptical Galaxies" (Eds. N. Arnoboldi, G.S. da Costa, P. Saha, 1997 PASP Conference Series Vol. 116), "Energy Transport in Radio Galaxies and Quasars" (Eds. P.E. Hardee, A.H. Bridle, J.A. Zensus, 1996 PASP Conference Series Vol. 100) and "Extragalactic Radio Sources" (Eds. R. Ekers, C. Fanti, L. Padrielli, 1996 IAU Symposium 175).

Figure 1. B-band image of NGC 5128 shows the traditional, almost circular inner part of the elliptical galaxy, crossed by a complex "dark band". The dark band is the projection of a strongly warped thin disk (Section 4). Note bright star clusters at the northwestern and southeastern edges of the band, and isolated dust clouds silhouetted against the stellar background. Supernova 1986g is the brightest of the two stars seen in the dark band about 45 mm from the left and 40 mm from the bottom. (Courtesy D. Malin, Ango-Australian Observatory)

1.2. Distance

With its great apparent brightness and galactocentric velocity of about $V_0 = +325\ km\ s^{-1}$, NGC 5128 is clearly a nearby galaxy. Early estimates of its distance ranged from 2.1 Mpc (Sersic 1958) to 8.5 Mpc (Sandage & Tammann 1974) and a "compromise" distance of 5 Mpc has frequently been used in the past. Many of the earlier distance values were derived by indirect means: group membership, redshift, comparison to Virgo cluster distance (assuming the latter to be known) etc. Summaries of the various distance determinations prior to 1993 can be found in Shopbell, Bland-Hawthorn & Malin (1993) and especially de Vaucouleurs (1993).

Attempts to use the occurrence of the SNIa supernova 1986g in NGC 5128 to derive its distance (Frogel et al. 1987; Phillips et al. 1987; Ruiz-Lapente et al. 1992) were frustrated by uncertainties in the internal reddening of NGC 5128 and in the absolute magnitudes of the supernova (see Sect. 3.3). It appears more useful to *assume a distance* to determine the supernova properties than the other way around. Other methods have been more succesful, consistently yielding a relatively nearby distance. The accuracies of these techniques were reviewed by Jacoby et al. (1992). Tonry & Schechter (1990) interpret the globular cluster counts by Harris et al. (1984a, 1986) to imply a distance modulus $(m - M)_0 = 27.53 \pm 0.25$ mag. Planetary nebula counts by Hui et al. (1993a) yield $(m - M)_0 = 27.73 \pm 0.14$. The lower value $(m - M)_0 = 27.48 \pm 0.06$ obtained by Tonry & Schechter (1990) from the surface brightness fluctuation of globular clusters must be revised to $(m - M)_0 = 27.71 \pm 0.10$ (Tonry 1991). Finally, Soria et al. (1996) estimate $(m - M)_0 = 27.72 \pm 0.20$ from halo red giant branch stars observed with HST/WFPC2. As there is no a priori preference for any of these methods, and as the weighted and unweighted averages of the various derived distance moduli are practically identical, the best value is thus $(m - M)_0 = 27.67 \pm 0.10$, corresponding to a distance of $D = 3.4 \pm 0.15$

Mpc. Note that at this distance, 1' on the sky corresponds almost precisely to 1 kpc. (2)

1.3. Systemic velocity

The systemic velocity of NGC 5128 is most frequently derived from measurements of components of the disk (Sect. 4). An overview of estimates up to 1984 can be found in Hesser et al. (1984); Table 1 lists all estimates **a.** later than 1975; **b.** having a quoted accuracy of 10 $km\ s^{-1}$ or better; and **c.** *not* based on HI or molecular line absorption (see Sect. 7). The estimates range from 536 to 551 $km\ s^{-1}$, and the mean is $V_{Hel} = 543 \pm 2\ km\ s^{-1}$.

Table 1. Systemic velocity estimates

Systemic Velocity	Obtained from:	Reference
V_{Hel} ($km\ s^{-1}$)		
548 ± 5	nebular emission lines	Graham (1979)
551.4	H α emission	Whiteoak & Gardner (1979)
541 ± 8	nebular emission lines	Rodgers & Harding (1980)
545 ± 5	H α emission	Marcelin et al. (1982)
538 ± 10	stellar absorption lines	Wilkinson et al. (1986)
536 ± 5	H α emission	Bland et al. (1987)
542 ± 7	HI emission	van Gorkom et al (1992)
541 ± 5	CO modelling	Quillen et al. (1992)
541 ± 7	PN emission lines	Hui et al. (1995)

1.4. Environment

Based on position and radial velocity, NGC 5128 is part of a group of 25 galaxies extending over about 25° on the sky (de Vaucouleurs 1975; Webster et al. 1979; Hesser et al. 1984; Côté 1995, 1997). In addition to NGC 5128, major members of the group are NGC 4945 and NGC 5236 (M 83) as well as the lesser NGC 5102, NGC 5253 and some twenty dwarf galaxies (Fig. 2). NGC 5128 is the only massive elliptical in the group. The group galactocentric velocity is very close to the individual velocities V_0 = 320-330 $km\ s^{-1}$ of the major members NGC 4945, NGC 5128 and NGC 5236 (Hesser et al. 1984). The members have an average projected radial distance to the centre of mass of 0.72 Mpc. The group has a crossing time of 5 gigayear and is probably still collapsing (Côté 1995, 1997). Assuming a distance of 3.4 Mpc, the group mass estimate by Hesser et al. (1984) becomes 5-17 × $10^{12}\ M_{\odot}$. It is quite remarkable that the other two major members, NGC 4945 and NGC 5236, as well as NGC 5253, exhibit signs of unusually vigorous star formation, while NGC 4945 also has a nuclear outflow. In addition, the dwarfs in the group have relatively high central surface brightnesses and exhibit clear star formation activity (Côté 1995).

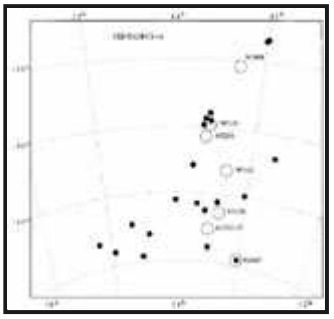

Figure 2. The Centaurus group of galaxies, with its brighter members identified. From Côté et al. (1997).

NGC 5128, itself a strong X-ray source (Sects. 2.4; 5.5), is surrounded by several X-ray point sources of a nature still unknown, although the majority of them seems to be associated with the galaxy (Arp 1994; Döbereiner et al. 1996).

---

[1] Useful photometric UBVR(I) sequences for NGC 5128 have been published by Graham (1980), McElroy & Humphreys (1982) and Zickgraf et al. (1990), reaching down to visual magnitudes of 16.6, 18.2 and 22.7 magnitudes respectively. Astrometric coordinates of field stars near the centre of NGC 5128 can be found in Griffin (1963). Very accurate field star positions and magnitudes may be obtained from http://astro.estec.esa.nl/SA-general/Projects/Hipparcos. Back.

[2] In the following all specific values quoted are reduced to D = 3.4 Mpc so that they may be different from the published values as given in the associated reference. Back.

2. THE RADIO SOURCE AND ASSOCIATED FEATURES

2.1. Overview

Owing to its proximity, Centaurus A (PKS 1322-427) is the largest extragalactic radio source in the sky. It extends predominantly in a north-south direction between declinations -38.5° $\leq \delta \leq$ - 46.5°, and between right ascensions $13^h15^m \leq \alpha \leq 13^h32^m$ (Fig. 3). Its overall angular dimensions are 8° × 4° (Cooper et al. 1965; Haynes et al. 1983; Junkes et al. 1993; Combi & Romero 1997). This translates into a linear size of 500 × 250 kpc. Although larger radio galaxies have been found (*cf.* Miley 1980), Centaurus A is still, in an absolute sense, one of the largest known. Its moderate radio luminosity places it in class I of the classification by Fanaroff & Riley (1974), suggesting only moderate relativistic beaming effects (Jones et al. 1994). For a recent study of the properties distinguishing FR-I and FR-II radio galaxies, see Zirbel (1996), and references therein.

The radio source is very complex; it shows significant structure ranging over a factor of 10^8 in size from the largest scales down to less than a milli-arcsecond. Major components of the radio source (see Fig. 3) are the giant outer lobes extending to 250 kpc, the northern middle lobe (no southern counterpart) extending to about 30 kpc, the inner lobes and central jets extending to about 5 and 1.35 kpc respectively and the compact core with associated nuclear jets extending over 1 pc (see Fig. 11).

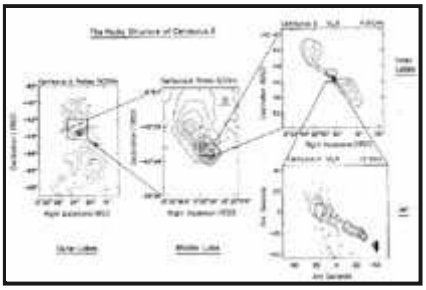

Figure 3. Radio maps of Centaurus A, highlighting the various components of the radio source introduced in Sect. 2.1. From Burns et al. (1983).

Table 2 provides a guide to radio continuum observations of Centaurus A. Part A lists radio continuum maps covering the *whole* source; integrated flux-densities are not always provided by the authors. Total source flux-densities between 85 MHz and 4750 MHz define an overall spectral index α = -0.6 (3) Part B refers to aperture synthesis radio maps of the bright inner part which comprises the inner lobes, jets and core, and single-dish maps at very high frequencies. References to other early single-dish maps and flux-densities at various frequencies can be found in Slee et al. (1983) and Tateyama & Strauss (1992). Part C, finally, summarizes radio images and flux-densities of the nuclear source. Very high resolution (VLBI) observations have shown a complex structure even for the inner few parsec which is further discussed in Sect. 5.4. Here, we draw attention to the high-frequency variability of the source which is clear from the Table and which is further discussed in Sect. 5.6.

Table 2. Radio continuum observations of Centaurus A

Reference	Frequency (MHz)	Resolution	Total Flux (Jy)

A. Whole Source			
Shain (1958)	20		28000
Sheridan (1958)	85		[a]7400
Cooper et al. (1965)	406	48'	2710
Haslam et al. (1981)	408	48'	
Bolton & Clark (1960)	960	20'	[a]1675
Cooper et al. (1965)	1410	14'	1330
Combi & Romero (1997)	1435	30'	
Cooper et al. (1965)	2650	7.4'	
Junkes et al. (1993)	4750	4.3'	681
Haynes et al. (1983)	5000	4.1'	
B. Inner Lobes & Core			
Slee et al. (1983)	327	55"	734
Slee et al. (1983)	843	40" × 60"	392
Christiansen et al. (1977)	1415	50" × 45"	215
Clarke et al. (1992)	1446	4.5" × 1.2"	78.3
Clarke et al. (1992)	1634	4.5" × 1.2"	63.5
Clarke et al. (1992)	4866	4.5" × 1.2"	37.5
Tateyama & Strauss (1992)	22000	258"	51.2
Tateyama & Strauss (1992)	43000	132"	31.2
C. Nucleus & Nuclear Jet			
Slee et al. (1983)	327	55"	2:
Slee et al. (1983)	843	40" × 60"	3:
Schreier et al. (1981)	1407	31" × 9.5"	3.4
Clarke et al. (1992)	1446	4.5" × 1.2"	3.7
Clarke et al. (1992)	1634	4.5" × 1.2"	4.9
Jones et al. (1994)	2300	0.1"	3.4
Schreier et al. (1981)	4866	31" × 9.5"	5.1
Clarke et al. (1992)	4866	1.1" × 0.3"	6.9
Jones et al. (1994)	8400	0.03"	5.9
Clarke et al. (1992)	14984	0.44" × 0.14"	9.4
Botti & Abraham (1993)	22000	252"	[b]16-32
Fogarty & Schuch (1975)	22000	252"	21.5
Kellerman (1974)	31500	225"	24
Tateyama & Strauss (1992)	43000	132"	10.8
Botti & Abraham (1993)	43000	132"	[b]7-20
Kellerman (1974)	89000	80"	18
Israel (unpublished)	89000	57"	[c]8
Israel (unpublished)	110000	47"	[c]7
Israel (unpublished)	145000	36"	[c]6

Notes: a. As revised by Cooper et al. (1965); b. Range of variation over period 1979 - 1992; c. Measurements in September 1996.

The whole radio source has been mapped with single-dish telescopes only, at linear resolutions no better than 4 kpc. The radio-bright inner lobes have been mapped with aperture synthesis telescopes at hundredfold higher resolutions of about 40 pc and the inner jets and core have been mapped at (sub)parsec resolutions in VLBI experiments. Aperture synthesis mosaicing of the outer features at substantially higher linear resolutions should be undertaken. Although a daunting task in view of the large angular sizes and low surface brightnesses, it is of great importance as no other radio galaxy allows its lobe structures to be studied in the detail possible in the case of Centaurus A.

2.2. The outer and middle lobes

The overall distribution of radio emission is roughly *S*-shaped. The distribution of radio emission across the *northern and southern outer lobes* is very asymmetric. The brightest part of the giant northern lobe is usually called the northern middle lobe; there is no such feature in the giant southern lobe for reasons that are not understood. One of the dwarf companion galaxies, UKS 1324-412 = ESO 324-G024, is seen in projection against the centre of the giant northern lobe. The isolated radio peak at $\alpha = 13^h18^m$, $\delta = -43°26'$ (Fig. 4) is not part of the southern lobe, but is due to a 15 mag background elliptical radio galaxy (Cooper et al. 1965; Haynes et al. 1983). This galaxy could be used as a tracer for conditions in the lobe (Junkes et al. 1993). Another unrelated dwarf galaxy, somewhat misleadingly known as the Fourcade-Figueroa Shred, is located at the tip of the southern main lobe (Dottori & Fourcade 1973). While radio surface brightnesses steadily decline away from the core in the northern lobe, they reach a maximum in the southern lobe at 1.8° from the core. The position angle of the northern lobe is close to 0°, while the southern outer lobe is displaced to the west and has a position angle of roughly 135°. The two lobes are connected by a low surface brightness "bridge" and the northern lobe is probably closer to us than the southern lobe (Junkes et al. 1993). Most of the emission from the lobes has a spectral index $-0.5 \leq \alpha \leq -0.7$, characterized by a ratio of random tc uniform magnetic field strength $B_r / B_0 = 0.6$ (Combi & Romero 1997). The outer lobes may be associated with hard X-ray limb brightening (Arp 1994).

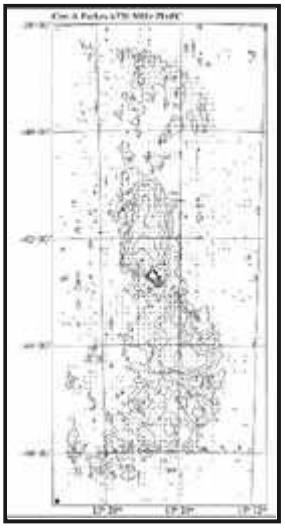

Figure 4. Radio map of Centaurus A at 4.75 GHz. Contours reach from 50 to 40000 mJy/beam area; HPBW beam size is 4.3'. E-vectors, marked for polarized intensities between 25 and 250 mJy/beam area, indicate both intensity and direction of polarization. The map shows the extent of the outer and middle lobes discussed in Sect. 2.2 . The inner lobes and jets, discussed in Sects. 2.3 and 2.4 are represented by the barely resolved strong double source in the centre. From Junkes et al. (1993).

The *northern middle lobe* is a major feature of the radio source: at 5 GHz it contributes almost 45% to the total radio emission from Centaurus A. Its overall orientation is north-south at $13^h23^m.5$ and it fades into the outer lobe at about δ = -41°30'. Its radio peak is at a projected distance of 20 kpc to the nucleus, at position angle 36° (Haynes et al. 1983). Whereas its radio intensities drop rather gently towards the north and northwest, its southeastern edge is relatively sharply delineated. The middle lobe is associated with soft X-ray emission, with a luminosity of about 5×10^{39} erg s^{-1} (Feigelson et al. 1981). Although inverse Compton scattering of the microwave background a priori is expected to occur in extended radio lobes, this explanation does not seem to fit the X-ray emission from this lobe (Feigelson et al. 1981 ; Marshall & Clark 1981 ; Morini et al. 1989). High-resolution radio observations - not yet existing - might enable a choice to be made between the remaining explanations of thermal and synchrotron emission.

The polarization E-vectors (perpendicular to the magnetic field direction) are well-aligned, but change their direction with increasing right ascension across the middle lobe from position angle $\approx$ 15° to 90°, emphasizing its concave southeastern boundary (Fig. 4; Junkes et al. (1993). Polarized intensities are between 20% and 40%, and the polarization from the middle lobe continues smoothly into that of the northern outer lobe where peak polarized intensities reach somewhat higher levels of up to 50% . The southern outer lobe has polarized intensity levels similar to those in the north, but south of δ = -44°30' its polarization structure abruptly becomes very chaotic. This could be due either to turbulence in the southern lobe, or to the presence of Galactic foreground polarization. Junkes et al. (1993) entertained the possibility that the giant northern lobe is bending into our line of sight, while the southern lobe may be turning away from the plane of the sky in the opposite direction.

In both lobes, steeper spectra are found where the radio surface brightness declines to low levels (see Fig. 4). These steep-spectrum regions appear to be unpolarized, but this may merely reflect a lack of sensitivity (Combi & Romero 1997 ; Junkes et al. 1993).

2.3. The inner lobes and outer jet

The two inner lobes (*cf.* Fig. 3) together contribute almost 30% to the total 5 GHz flux-density of Centaurus A. The radio emission from the northern inner lobe is about 40% higher than that from the southern inner lobe. Slee et al. (1983) show that both lobes have identical nonthermal spectral indices α = -0.7, and estimate from this an age of 6×10^8 years.

With a maximum angular size of 12', the inner lobes are usually not, or poorly, resolved by single-dish telescopes. Aperture synthesis maps (Fig. 5) reveal pronounced filamentary structure especially in the southern lobe, probably generated by velocity shear in the turbulent flow of the lobe rather than by shocks (Clarke et al. 1992). The northern lobe has a fairly sharply delineated southeastern edge. At the same position angle as the inner lobes, Arp (1994) has found a jet of diffuse X-ray emission, extending, however, much beyond northern radio lobe limits. Its nature and origin are not clear. No soft X-ray emission is seen towards the inner lobes (Feigelson et al. (1981).

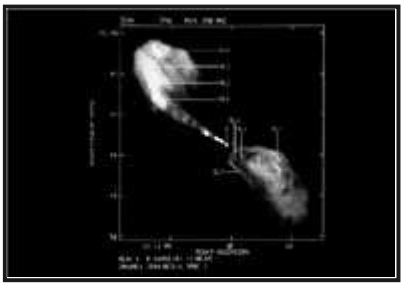

Figure 5. Gray scale 5 GHz image of the inner lobes and jets of Centaurus A at a resolution of 4.4 × 1.2 arcsec. The gray scales range linearly from -3.0 mJy per beam (dark) to 35.0 mJy per beam (light). The labelled features are discussed in Clarke et al. (1992). Courtesy J. Burns, Univ. of Missouri-Columbia).

In the high-resolution maps shown by Clarke et al. (1992), the inner lobes are revealed as subsonic plumes emanating from a supersonic central jet at a position angle of 51°. The jet-lobe transition occurs at the location of the innermost optical shell identified by Malin et al. (1983) and marked No. 9 in Fig. 7 . This transition has been interpreted as evidence for shock disruption of the jet at the interface of the interstellar and intergalactic medium of the galaxy (Norman et al. 1988 ; Gopal-Krishna & Saripalli 1984).

The northern jet is quite pronounced and shows several knots, whereas the southern (counter)jet was first surmised from the detection of a few weak knots in the southern lobe (Clarke et al. 1986; 1992); it is now confirmed by VLBI images (Sect. 5.4). The direction of polarization in the inner lobes is dramatically different from that in the middle and outer lobes. Beyond the sharply delineated northern plume perimeter, at a projected distance of 6.3 kpc to the nucleus, it changes abruptly by 90°, so that the northern inner lobe is quite distinct from the middle lobe. E-vector alignments indicate a magnetic field emanating radially from the nucleus along the lobe axis; at the edges of both lobes, the magnetic field is parallel to the plume perimeter (Clarke et al. 1992). At 5 GHz, both lobes are $\approx$ 35% polarized with some regions having polarizations as low as 15% or as high as 50%. The southern lobe is more strongly depolarized, most likely because it is located behind the clumpy interstellar medium of the galaxy's disk component (Sect. 4). It exhibits a much less ordered polarization pattern (Clarke et al. 1992; Junkes et al. 1993).

Broad-line high excitation gas appears to be associated with the inner lobes, but its nature is still unclear (Phillips et al. 1984 and references therein).

2.4. Inner jet structure

The morphologies of the inner radio jet (Schreier et al. 1981) and the X-ray jet (Schreier et al. 1979; Feigelson et al. 1981; Döbereiner et al. 1996; Turner et al. 1997) are very similar. They fill the gap between the nucleus and the optical filaments reported by Dufour & van den Bergh (1978 - Sect. 2.5). Seven major concentrations (usually labelled A through G following Feigelson et al. 1981) can be discerned with rather identical radio/X-ray flux ratios. The knots are brightest nearest the nucleus and are separated by typically 30". They have 0.4-4.5 keV X-ray luminosities of $0.2\text{-}1.0 \times 10^{39}$ erg s^{-1}. Once again, it appears that inverse Compton radiation cannot explain their nature, although both thermal and synchrotron models are possible (Feigelson et al. 1981; see also Turner et al. 1997). The kinetic energy of the jet averaged over time exceeds the radiative energy of the nucleus. It has been suggested that both radio and X-ray emission are produced by a single population of relativistic electrons with Lorentz factors $\gamma \approx 8 \times 10^7$ in 60 microgauss magnetic fields (Schreier et al. 1981; Burns et al. 1983). As such electrons have lifetimes of 50 years or less, in any event much shorter than light travel times *even across the knots*, this requires in situ acceleration (Schreier et al. 1981; Feigelson et al. 1981; Burns et al. 1983; Turner et al. 1997). There is no evidence for X-ray flux variations of the *inner jet* (Döbereiner et al. 1996; Turner et al. 1997), in contrast to the *nuclear jet* (see Sect. 5.6).

High resolution radio images (18 × 5 pc) by Clarke et al. (1986; 1992) illustrate the extremely inhomogeneous nature of the main (northern) jet, with a hierarchy of knots reaching down to sizes less than 2.5 pc. The jet is not a linear structure, but exhibits side-to-side limb brightening, perhaps due to a combination of external and internal shocks (Clarke et al. 1986). As most of the jet is inside the main body of the galaxy, some degree of interaction with the gaseous medium of the galaxy is to be expected. Indeed, Burns et al. (1983) suggested that the inner jet is confined by external pressure. In the knots, the spectral index decreases from α = - 0.7 at the limb-brightened side to α = - 1.4 at the diffuse side, while polarized fractions drop from 40% to less than 20% . Filaments or streamers connect knot complexes to ones downstream; they have steep spectra α = - 1.4. If the knots are shock fronts reaccelerating electrons, the streamers will represent material flowing down the jet away from these fronts at speeds of 5000 *km* s^{-1}; the spectral steepening reflects increasing importance of synchrotron energy losses (Burns et al. 1983; Clarke et al. 1986).

2.5. Optical jet features

Intense optical emission from the knots in the brightest part of the X-ray/radio jet, at 0.25'-1.0', and also from in between the knots, was discovered by Brodie et al. (1983). The emission is due to gas at densities of a few hundred per cc in the knots, and from gas at less than 10 per cc in the interknot region. At least one of the optical features corresponds precisely to radio/X-ray structure suggesting shock excitation of clumps carried along in the jet flow. The continuum appears to be the optical counterpart of the synchrotron X-ray/radio emission (Brodie & Bowyer 1985).

Somewhat farther out, a long chain of filaments, dust clouds, H α knots and blue stellar objects emanates from the centre of the galaxy more or less along the direction of the jet. This chain starts at about 2' from the nucleus and extends out to 28' (see the review by Danziger 1981 and references therein). It breaks up into three distinct groups of features.

The socalled *inner jet structures* of this chain are found between 2' and 6' (Dufour & van den Bergh 1978); the features closest to the nucleus are aligned with but offset from the radiojet, just where this starts to develop in the plume of the northern inner lobe. The outermost features of this group continue at the same position angle, although the radio plume expands away to the north. In their Fig. 1, Morganti et al. (1991) provided high-quality images as well as a very useful diagram of the relative positions of optical and radio structures. The next group out (commonly called the *inner filaments*) occurs between 8' and 10' from the nucleus at the same position angle as the jet (*PA* = 55°), although the outermost may start "veering off course" (see Morganti et al. 1992). They are easily visible on long-exposure images of NGC 5128 (*cf.* Figs. 6 and 7). These filaments are in the northern middle radio lobe, but have no known specific radio counterpart. This may reflect the lack of high-resolution radio images of the middle lobe more than anything else and provides another rationale for obtaining such. The filaments have very

high [OIII] / H β ratios of about 15 and are blueshifted by up to 400 *km* s^{-1} from the systemic velocity of the galaxy (Osmer 1978; Morganti et al. 1991). They consist of turbulent low-density gas and coincide with the soft X-ray emission associated with the northern middle lobe (Feigelson et al. 1981; Graham & Price 1981; Graham 1983).

The *outer filaments* (at 17.5') are also in the middle radio lobe, again without obvious radio counterpart at least at the low resolutions presently available. Their position angle, *PA* = 43° is markedly different from that of the other filaments (Fig. 6). In addition to the brightest main filaments, there are weaker features to the north and west. Graham (1983) measured some rather high blueshifts up to 1000 *km* s^{-1}, but Morganti et al. (1991) found blueshifts of only 70-215 *km* s^{-1} for the main filaments.

The origin and excitation of the filaments has been a matter of some debate. Although some of the features have spectra similar to those of "normal" HII regions, several (notably the inner filaments) have spectra suggesting photo-ionization by a (nuclear) power-law spectrum or by shock excitation. Metallicities appear to rule out a primordial origin of the gas. The filaments may be formed by the expanding radio lobes compressing ambient gas to temperatures of a few million K followed by rapid cooling on a timescale of 10 million years (Feigelson et al. 1981; Gouveia dal Pino & Opher 1989). Alternatively, the jet may consist of material ejected from the nuclear region (Graham & Price 1981), although it is questionable whether this would survive long enough to have reached the presently observed distance to the nucleus (Graham 1983). In a rather extensive study of the filaments, Morganti et al. (1991, 1992) concluded that they are predominantly photoionized by the radiation from the nucleus itself, extinguished in our line of sight but travelling unimpededly along the jet. They proposed that a BL Lac nucleus lies at the core of Centaurus A. This conclusion was tentatively supported by Schiminovich et al. (1994) who found that the apparently counterclockwise rotating HI clouds near these filaments have velocities very similar to those found optically. However, Viegas & Prieto (1992) argued that additional heating mechanisms are required, and suggested the presence of shocks. They also concluded that a mixture of optically thin and optically thick gas is necessary for photoionization to be a viable explanation. In contrast, Sutherland et al. (1993) proposed that instead of photo-excitation, the mechanical flux of a mildly supersonic low-density jet interacting with dense ambient clouds is sufficient to energize shock waves with velocities $\approx$ 200-450 *km* s^{-1}. Their model reproduces several observed features of the filaments, and removes the need for a narrow ionizing beam as proposed by Morganti et al. (1991, 1992). As the latter model predicts strong UV line fluxes from the filaments, whereas the former does not, such an observational test would be interesting.

Finally, we note that the inner filaments are at the same position angle as the inner jets, the more distant outer filaments are at the same position angle as the bright NL-2 component (Clarke et al. 1992; see Fig. 5) in the plume, and the even more distant faint galaxy extensions in Fig. 8 line up with the NL-4 component in the plume (see Fig. 5). Whether this is accidental, or provides clues to their origin is unclear.

---

[3] Spectral index α is defined by $S_\nu \propto \nu^\alpha$ Back.

3. THE GALAXY

3.1. Overview

With *V* = 6.98 mag (de Vaucouleurs et al., 1976 - RC2), NGC 5128 is the fifth brightest galaxy in the sky, immediately after the Local Group members M 31, M 33, LMC and SMC. Images of relatively short exposure, limited to a surface brightness in B of about 22 mag per arcsec^2, show an almost circular appearance, which has led to the classification S0p or E0p (Fig. 1). However, at lower surface-brightness levels (Fig. 8), the shape of the galaxy becomes increasingly noncircular. At about 25 mag per arcsec^2, the axial ratio has increased to 1.3, after which elliptical symmetry is lost (*cf.* Haynes et al. 1983). A more appropriate classification appears to be E2 (Dufour et al. 1979; McElroy & Humphreys 1982; Haynes et al. 1983; Ebneter & Balick 1983), with the photometric major axis of the galaxy at position angle 35°. The light distribution closely follows the $r^{1/4}$ de Vaucouleurs law (van den Bergh 1976) characteristic of elliptical galaxies. The inner parts of NGC 5128 have a roughly constant total mass-to-light ratio inccreasing with radius, probably due to the presence of dark matter (Sect. 6.2).

Of particular interest are the deep and specially processed optical images presented by Malin et al. (1983 - see Fig. 6) and Haynes et al. (1983 - see Fig. 8). The former reveals an extensive system of shells of old disk stars within the extended elliptical galaxy. The system is most regular on the northeastern side, and more fragmented on the southwestern side. The outermost shell is found at 18' from the nucleus. Atomic neutral hydrogen emission with a total mass of 1.5×10^8 $M_\odot$ is present just outside several of the outer shells (Schiminovich et al. 1994), with a rotation axis at position angle 285°, somewhat offset from the

position angle of the minor axis of the E2 galaxy and the dust band (Fig. 7).

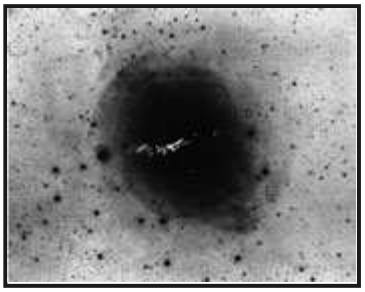

FIgure 6. Deep negative B-band image of NGC 5128 shows the system of optical shells at the edges of the galaxy. This system of shells is one of the clearest indications that NGC 5128 has undergone mergers in its past. Also note optical jet features at a position angle of about 45°, inside and outside the northeastern shells respectively. Courtesy D. Malin, Ango-Australian Observatory)

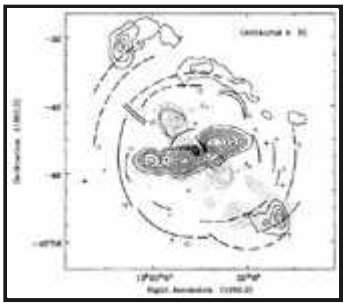

Figure 7. Contours of total HI superposed on a schematic image of the shells of NGC 5128. Contours reach from 1 to 40 × 10^{20} cm^{-2}. Thick lines mark the position of sharp (solid) and diffuse (dashed) shells. Shaded regions represent dust patches. Thin contours marked A_n and A_s represent the radio continuum emission from the inner lobes and jets discussed in Sects. 2.3 and 2.4. Most of the neutral hydrogen is associated with the warped disk discussed in Sect. 4, but some of it is associated with the shells (Sect. 3.1). From Schiminovich et al. 1994 ; image courtesy J.M. van der Hulst.

The image presented by Haynes et al (1983; see also Cannon 1981) shows diffuse extensions emanating from the elliptical galaxy at position angle $\approx$ 30° almost perpendicular to the major axis of the dusty disk in the centre (Fig. 8). The northeastern extension is narrower, longer and better-defined than the one in the southwest. It is just west from the northern middle radio lobe. The faint extensions most likely consist of stars, or possibly of dust reflecting light from stars further in (Cannon 1981; Haynes et al. 1983).

Figure 8. Very deep, amplified positive B-band image of NGC 5128 shows the elongated structure of the galaxy, as well as faint emission extending roughly along the direction of the inner radio jets. The "traditional" negative image of NGC 5128 has been superposed for comparison. The dark band is clearly inside the galaxy. From Haynes et al. 1983; image courtesy D. Malin, Ango-Australian Observatory).

The appearance of NGC 5128 departs strikingly from that of a normal elliptical galaxy because of its broad and patchy equatorial dark band. Bisecting the almost circular bright central part of the galaxy, it is oriented along the *minor axis* of the elongated shape seen in deep images (Fig. 8). Consequently, NGC 5128 is sometimes also classified as a polar ring galaxy although it fails to share several of the characteristics common to these (see Richter et al. 1994). The dark band is associated with young stellar objects (Dufour et al. 1979 - see also Fig. 6). Modelling has shown that it is in fact a *thin*, strongly warped disk embedded in the host galaxy that creates the superficial appearance of a broad band (Sects. 4 and 6). Kinematically, the galaxy and the dark band represent different entities. The elliptical system and its globular cluster retinue have low rotational velocities, whereas the dust disk exhibits much higher rotational velocities (Sect. 6.1).

3.2. Globular clusters and metallicity

The galactic foreground confusion caused by the low galactic latitude (b = +19°) of NGC 5128 for a long time impeded attempts to identify its globular clusters, notwithstanding its proximity. However, after the first identifications were finally made by Graham & Phillips (1980) and van den Bergh, Hesser & Harris (1981), the number of confirmed globular clusters rose steadily from 20 (Hesser et al. 1984) to 35 (Hesser, Harris & Harris 1996) to 87 (Harris et al. 1992) while Minitti et al. (1996) added another 26 globular clusters in the inner 3 kpc of the galaxy. Analyzing image counts, Harris et al. (1984a) have estimated a total cluster population of 1550 ± 350. Globular cluster studies have been used primarily to extract information on the galaxy's metallicity and dynamics, as well as its distance (Sect. 1.2). In terms of both numbers and metallicities, the globular cluster system of NGC 5128 appears to be normal for large elliptical galaxies (Harris et al., 1984b, 1992) or indeed for spheroidal components of galaxies in general (Jablonka et al. 1996).

At least at radii beyond 4', the surface density of globular clusters appears to follow the same $r^{1/4}$ law as found by van den Bergh (1976) for the spheroidal halo light. In addition, the distribution of globular clusters on the sky hints at a preferential orientation, with a major axis aligned with the major axis of the outer isophotes of NGC 5128 (Hesser et al. 1984). Although the first determinations of very high metallicity by Frogel (1984) turned out to be overestimates, the clusters in NGC 5128 do seem to have somewhat greater metallicities ($-0.6 \leq [Fe/H] \leq +0.1$) than their Milky Way counterparts which they otherwise resemble (Harris et al. 1992; Jablonka et al. 1996; Minniti et al. 1996; Alonso & Minniti 1996). Rather similar metallicities were derived for red giant branch stars by Soria et al. (1996). The innermost clusters are on average more metal-rich, implying the presence of a metallicity gradient $\Delta [Fe/H] / \Delta R$ = -0.08 dex kpc^{-1}; this gradient is only apparent, and in fact caused by *differen concentrations* of metal-poor and metal-rich clusters (Alonso & Minniti 1996, but see Jablonka et al. 1996).

Half a dozen of the innermost clusters have magnitudes and colours (but undetermined metallicities) suggesting that they are intermediate-age clusters such as found in the Magellanic Clouds (Minniti et al. 1996; Alonso & Minniti 1996). Hui et al. (1995) showed that the metal-poor globular cluster ensemble lacks significant rotation whereas the metal-rich ensemble rotates more rapidly. A puzzling, but still uncertain result was obtained by Hesser et al. (1986). They found that the metal-rich innermost

cluster ensemble has a mean velocity about a 100 $km\ s^{-1}$ (4 σ) higher than the systemic velocity of NGC 5128, in contrast to the outermost clusters that conform to the systemic velocity.

The bimodal globular cluster population of NGC 5128 is of great interest in view of the proposed merger-nature of the galaxy, particularly as a bimodal metallicity distribution with metal-rich clusters more concentrated than metal-poor clusters has been identified by Zepf & Ashman (1993) as the natural consequence of galaxy mergers.

3.3. Late-type objects

A survey of [OIII] λ5007 emission from planetary nebulae in NGC 5128 by Hui et al. (1993a), extending over 20 kpc along the major axis and fully covering the central 10 kpc, yielded 785 detections (Hui et al. 1993b). The high-luminosity cut-off of the resulting PN luminosity function was used to derive the galaxy distance in Sect. 1.2. Hui et al. (1995) measured radial velocities for 433 PN's, which were used to study the kinematics and dynamics of the galaxy (Sect. 6.2).

A V-I colour-magnitude diagram of 10000 red giant branch (RGB) stars in the halo of NGC 5128 was constructed by Soria et al. (1996) from HST/WFPC2 images, the first time that individual stars were resolved in a spheroid system beyond the Local Group. Analysis of the results yielded the distance and metallicity values already mentioned (Sects. 1.2 and 3.2). The I-luminosity function of these stars is very similar to that of the RGB stars in the M 31 dwarf elliptical companion NGC 185. About 200 stars were found to be brighter than the tip of the RGB; most of them are probably upper asymptotic giant branch (AGB) stars although confusion with unresolved multiple stars is still a problem. The luminosity functions of these AGB stars suggest the presence of an intermediate-age population of about 5 gigayear, but making up at most 10 % of the total halo stellar population.

Over the five-year period 1985-1989, Ciardullo et al. (1990) monitored NGC 5128 for the appearance of novae. They detected 16 novae, twelve of which formed a statistically complete and homogeneous sample unaffected by the dust lane. Normalized to the near-infrared K-band luminosity, the derived nova rate of 4.2 yr^{-1} per $10^{10}\ L_K$ is virtually identical to that derived for the bulge of M 31. They further argued that the normalized nova-rate of galaxies is largely independent of their luminosity, colour or Hubble type.

The galaxy was the host of the type Ia supernova 1986g (Evans 1986), which reached a maximum at B = 12.45 ± 0.05 (Cristiani et al. 1992). With A_B = 4.4 mag and the currently best value for the distance modulus, this translates into an absolute magnitude M_B = -19.6 ± 0.5. However, the reddening of SN 1986g, mostly caused by dust internal to NGC 5128, is variously given as $E(B - V)$ = 0.9 (Phillips et al. 1987), 1.1 (Cristiani et at. 1992), 0.6 (Phillips 1993) and 1.6 (Hough et al. 1987). The latter also argued from their polarization measurements that near SN 1986g the ratio of total to selective extinction R is 2.4, rather than 3.1. The resulting A_V values thus range from 1.9 to 3.8 mag, so that the extinction correction remains a major source of uncertainty. This could be resolved by assuming an SNIa mean peak absolute magnitude. Unfortunately, estimated values range from M_B = -19.75 (Cristiani et al. 1992), -19.4 (Branch et al. 1996) to -18.2 (Phillips 1993), the major uncertainty this time being galaxy distance moduli. A further discussion of the use of SNIa's as standard candles is outside the scope of this review; for recent contributions see e.g. Riess, Press & Kirshner (1996) and Branch, Romanishin & Baron (1996).

3.4. Colours and reddening

The integrated colour of NGC 5128 as given in the RC2 is $(B - V)_T$ = +0.98. This is identical to the colour van den Bergh (1976) finds at distances of 150" to the dark band centerline, where also $(U - B)$ = +0.49. The foreground reddening is $E(B - V)$ = 0.11 ± 0.02 (Newell et al. 1969; Frogel 1984; Harris et al. 1992), so that the intrinsic colours become $(B - V)_0$ = 0.88 and $(U - B)_0$ = 0.41, bluer by 0.08 mag resp. 0.15 mag than normal for elliptical galaxies (van den Bergh 1976). The photometry by van den Bergh shows *increasing blueness* approaching the dark band; at its edge, 40" from the centerline, the colours abruptly spread over a great range +0.4 $\leq (B - V) \leq$ +1.2 and -0.6 $\leq (U - B) \leq$ +0.5, whereas in the dark band only *red colours* are found (+1.0 $\leq (B - V) \leq$ +1.6; +0.3 $\leq (U - B) \leq$ +0.9). The excess blue emission has been explained as due to optical synchrotron emission from the inner lobes (Dufour et al. 1979), a metal-poor population, or a young population of hot, blue stars. The first explanation is unlikely (Ebneter & Balick 1983), as is the second in view of the metallicity results given in Sect. 3.2, particularly those by Soria et al. (1996). The last explanation is supported by the presence of a substantial number of HII regions in the dust band itself (Dufour et al. 1979 ; Hodge & Kennicutt 1983), and even more so by colour images of the galaxy that show substantial very blue stellar populations at the northwestern and southeastern edges of the dust band (*cf.* Fig. 1).

A much less sharply delineated and less extreme increase of blue colours occurs farther out, in the inner halo, and probably reflects the increasing presence of metal-poor objects (van den Bergh 1976).

4. The dusty disk

4.1. Overview

Dufour et al. (1979) first established that the dark band crossing the elliptical galaxy is in fact the image of a highly inclined *disk component* consisting of a metal-rich population of stars, nebulae and dust clouds (Fig. 1). Metallicities are close to those in the Solar Neighbourhood (Dufour et al. 1979; Phillips 1981; Eckart et al. 1990a; Viegas & Prieto 1992). The disk is at position angle 122° ± 4° and star formation is rampant. The present burst of star formation apparently started 50 million years ago and created at least a hundred HII regions embedded in the disk (Dufour et al. 1979; Hodge & Kennicutt 1983). Remarkable concentrations of luminous and very blue stars can be seen at the northwestern and southeastern edges of the dark band; they must represent very large OB associations (Fig. 1). Recent HST observations allowed Schreier et al. (1996) to also find a large number of point-like sources *embedded in* the dust band with colours likewise suggestive of OB associations (see also Alonso & Minniti 1997). However, since the review by Ebneter & Balick (1983), little quantitative progress has been made on the issue of star formation. This may occur at rates ten times higher than in the Milky Way (Telesco 1978) although disk average UV energy densities close to Solar Neighbourhood values (Eckart et al. 1990a) suggest more moderate rates.

As NGC 5128 is no more distant than e.g. M 82, its brightest HII regions and supernova remnants should be detectable at centimetre radio wavelengths. Most of the published high-resolution radio maps lack the dynamic range to reach the low flux-density levels expected for HII regions or SNR's in the disk. The 1425 MHz map published by Condon et al. (1996) does, however, show an extension with peaks of 125 mJy in an 18" (295 pc) beam coinciding with the eastern half of the dark band, while the 43 GHz map by Tateyama & Strauss (1992) likewise seems to show weak emission from the eastern dark band. Further high-resolution observations of the disk at centimetre wavelengths are desirable as they provide one of the few means studying the star formation history of the disk.

As defined by its OB stars and HII regions, the disk extends out to a radius of 4 kpc. Molecular line and infrared continuum emission, further discussed in Sects. 4.2 and 4.3, is concentrated within 40% of this radius (Joy et al. 1988; Eckart et al. 1990a; Quillen et al. 1992). HI emission, however, extends much farther out, to radii of 7 kpc (*cf.* van Gorkom et al. 1990; Schiminovich et al. 1994). The outer parts of the disk, as traced by the dark band and the HI emission, show a pronounced warp to position angle 90° (*cf.* Fig. 7). The disk is in rapid rotation (Graham 1979; van Gorkom et al. 1990; Quillen et al. 1992). The tilted-ring modelling by Nicholson et al. (1992) shows that in spite of appearances, the distribution of dust in NGC 5128 is that of a warped *thin disk* of about 200 pc thickness (Sect. 6.1) along the minor axis. Deep images of NGC 5128 show the disk to be well inside the elliptical galaxy. Its inclination is a function of radius, but remains generally high with respect to the plane of the sky. The HII regions are distributed throughout the warped disk and embedded in diffuse ionized gas. Nicholson et al. (1992) showed that their warped disk model also quite naturally explains the various CaII and NaI velocity components seen in absorption against supernova 1986g by d'Odorico et al. (1989). In addition to the seven components associated with NGC 5128, these observationsy also showed three components with Galactic foreground gas, and two intermediate velocity components of unknown origin.

The inner part of NGC 5128 is associated with diffuse X-ray emission in the form of ridges along the dark band edges but also in more isotropically distributed form (Feigelson et al. 1981; Turner et al. 1997). Although the origin of this diffuse emission is not established unequivocally, among the most reasonable explanations for its existence are gas ejected from late-type stars dynamically heated to the required temperatures, X-ray binaries associated with the young stellar population, stellar winds in HII regions or combinations thereof (Feigelson et al. 1981; Turner et al. 1997). In any case, NGC 5128 is underluminous in diffuse X-ray emission as compared to other early-type galaxies (Döbereiner et al. 1996).

4.2. Atomic and molecular gas

The HI observations by van Gorkom et al. (1990) and Schiminovich et al. (1994) show the atomic hydrogen to follow the dust lane, including the warp (Fig. 7). It could, however, not be traced over the central 2.5 kpc because of strong absorption against the centre. Van Gorkom et al. (1990) found a total HI amount of about $3.3 \times 10^8\ M_\odot$, but cautioned that they might have missed a significant amount because of limited sensitivity; nor does this estimate include the HI in the shells found by Schiminovich et al. 1994 (Fig. 7). Indeed, Richter, Sackett & Sparke (1994) find within the 21' (21 kpc) beam of the Green Bank 140 ft telescope a higher mass of $8.3 \pm 2.5 \times 10^8\ M_\odot$, still uncertain because of the strong central absorption (Sect. 7).

In the central part of the disk, molecular line emission from CO and its isotopes is found out to radii of about 2 kpc, but most of it is concentrated within a radius of 1 kpc (Phillips et al. 1987; Eckart et al. 1990a; Quillen et al. 1992; Rydbeck et al. 1993). Within R = 1 kpc, the area filling factor of the disk is of the order of 3-12%, its thickness is less than 35 pc and the velocity dispersion is about 10 $km\ s^{-1}$ (Quillen et al. 1992). The J = 2-1/J=1-0 temperature ratios of about 0.9 for both ^{12}CO and ^{13}CO as

well as the isotopic emission ratios ^{12}CO / ^{13}CO = 11 and ^{12}CO / C^{18}O = 75 are comparable to those of Milky Way giant molecular cloud complexes (Wild, Eckart & Wiklind 1997). Modelling the CO observations as tracer for the much more abundant H_2 molecule, Eckart et al. (1990a) and Wild et al. (1997) estimate molecular hydrogen temperatures T_k = 10-15 K and densities of a few times 10^4 cm^{-3}. Emission from other molecular species has also been detected in the disk (Whiteoak, Gardner & Höglund 1980; Seaquist & Bell 1988; d'Odorico et al. 1989; Israel 1992; Paglione, Jackson & Ishizuki 1997).

Total molecular hydrogen masses are probably about 4×10^8 $M_\odot$, but may be a factor of two higher depending on the CO-to-H_2 conversion factor favoured. The vibrationally excited warm H_2 ($T_k \approx$ 1000 K) detected by Israel et al. (1990) represents only a minute fraction of all molecular hydrogen and is associated with the circumnuclear disk (Sect. 5.2). The total gaseous mass of the disk, including helium, is thus of the order of 1.3×10^9 $M_\odot$, only about 2% of the dynamical mass contained in the elliptical component within the radius of the disk (R = 7 kpc). However, because of the pronounced concentration of interstellar gas at smaller radii, that fraction increases to about 8% at R = 2 kpc.

4.3. Dust emission

At far-infrared wavelengths, the disk of NGC 5128 stands out by its emission from warm dust. Dust temperatures are 30-40 K depending on the assumed dust emissivity $Q_{100} \propto \lambda^{-2}$ or λ^{-1} respectively (Joy et al. 1988; Marston & Dickens 1988; Eckart et al. 1990a). The overall distribution of far-infrared emission is very similar to that of the carbon monoxide. The present far-infrared information still leaves considerable room for improvement. The KAO scans presented by Joy et al. (1988) do not fully sample the galaxy, but show that 10% of the total far-infrared luminosity arises in central source which may be identified with the circumnuclear disk (see Sect. 5.2). IRAS survey observations cover the whole galaxy, but the resolution is limited. Several of the published fluxes refer to poorly calibrated data or underestimate the total flux from the extended galaxy. Best fluxes are probably the colour-corrected values S_{12} = 26.4 Jy, S_{25} = 25.7 Jy, S_{60} = 236 Jy and S_{100} = 520 Jy given by Rice et al. (1988). Use of IRAS non-survey data (DSD maps: Marston & Dickens 1988; CPC-maps: Eckart et al. 1990a; Marston 1992) provided some improvement in resolution, but at the cost of photometric accuracy. Because of unsolveable calibration problems (*cf.* van Driel et al. 1993), the image-sharpened CPC maps discussed by Eckart et al. (1990a) and by Marston (1992) must be considered as unreliable. The most recent image-sharpened IRAS maps (resolution 1-2') incorporating all survey-instrument data are shown in Fig. 9; they still lack the resolution to bring forth the full detail of the disk.

Good mid-infrared imaging of the dust disk itself is still lacking. The mean 12μm surface brightness of the disk as derived from IRAS data is about 25 MJy sr^{-1}. In addition to the nucleus (Sect. 5.3), Telesco (1978) detected 10μm emission weaker by a factor of about five from a number of disk HII regions. Clearly, much more remains to be done.

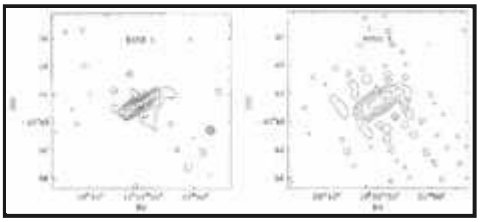

Figure 9. IRAS image-sharpened maps of the NGC 5128 dusty disk at 12μm (Band 1) and 60μm (Band 3), showing the warped outer edges. Courtesy D. Kester, University of Groningen.

As much as 50% of the 100μm emission may be due to "cirrus" (Marston & Dickens 1988; Eckart et al. 1990a). The various far-infrared data indicate the presence of small amounts of dust outside the disk in the main elliptical galaxy as well as large amounts in the disk out to a radius of 3 kpc (Eckart et al. 1990a; Marston 1992). The total dust mass can be estimated from IRAS photometry as M_d = 1-2 $\times 10^6$ $M_\odot$ (*cf.* Hunter et al. 1989) with a luminosity $L_{FIR} = 2 \times 10^{10}$ $L_\odot$ (Joy et al. 1988; Eckart et al. 1990a). With considerable uncertainty, the *total* gas-to-dust ratio within a radius of 2 kpc is M_{gas} / M_{dust} = 450. This is an upper limit if significant amounts of cold dust are present, imperfectly sampled by IRAS. Marston & Dickens (1988) explicitly modelled the IRAS emission in terms of large, cool grains and warm, small grains, and arrived at a (distance-corrected) dust mass an order of magnitude higher, implying a gas-to-dust ratio of 45, which seems rather low.

4.4. Polarization and extinction

At optical and infrared wavelengths, the disk is significantly polarized up to 6% parallel to the dust band (Elvius & Hall 1964; Hough et al. 1987; Scarrott et al. 1996). The observations by the latter show higher levels of polarization at the dust band extremities, with directions perpendicular to the dust band. Hough et al. (1987) concluded that the dust grains sampled are about 20% smaller than those in the Milky Way, implying an extinction law differing from that in the Solar Neighbourhood, with a total to selective extinction ratio of 2.4. The HST R- and I-band imaging polarimetry presented by Schreier et al. (1996) shows the polarization to reach a peak at a knot close to the nucleus, shining by reflected light. Like Hough et al. (1987), they assumed scattering to be negligible elsewhere, but that is inconsistent with the apparent importance of scattering in the central region and is unlikely in view of the conclusions reached by Packham et al. (1996 - see Section 5.3). The observations by Scarrott et al. (1996) can only be explained by assuming simultaneous operation of both dichroic extinction and scattering, with the latter dominating at the dust band extremities. This suggests that the very blue colours observed by van den Bergh (1976) just at the *northern* dark band edge are caused by the light of intrinsically blue objects (*cf.* Alonso & Minniti 1997 and references therein) enhanced by scattered light and suffering relatively little extinction. This is supported by the optical continuum observations of the central region by Storchi-Bergmann et al. (1997) who find that the major contribution comes from a metal-rich old bulge, but that there are also significant contributions from young stars and from scattered light especially at the dark band edges.

The optical colours suggests significant extinction in the dust band itself ($E(B - V) \geq 0.5$ mag - van den Bergh 1976; Dufour et al. 1979). Indeed, the near-infrared estimates by Harding et al. (1981) yield A_V = 3-6 mag, while HST observations indicate V-band extinctions ranging from 0.5 to 7 mag in the dark band (Schreier et al. 1996) and even reaching values in excess of 30 mag ($A_K \geq 3$ mag) just south of the optically invisible nucleus (Alonso & Minniti 1997). The R-band and I-band images by Schreier et al. (1996) clearly show how the dust band is seen nearly edge-on, but slightly tilted with the near side south of the centre so that we are looking from above. The glow of the nuclear region (but not the nucleus itself) on the north-side of the dust disk is strikingly apparent even through the high extinction it suffers.

5. THE CENTRAL REGION

5.1. Overview

The central region of the galaxy, within a few hundred parsec from the nucleus, is very complex. The nucleus itself, hidden behind thick dust clouds, is visible at infrared (Sect. 5.3), (sub)millimetre and centimetre wavelengths (Sect. 5.4) and again at high energies (Sect. 5.5), but generally requires very high resolutions to separate it from its surroundings. At centimetre wavelengths and at high energies, confusion is caused by the emission from the inner jet and even more so from the milliarcsec nuclear jets (Meier et al. 1989; Jones et al. 1996; Tingay et al. 1998). With increasing observing frequency, the steep nonthermal spectrum of the jet features reduces them to insignificance, so that shortwards of 1 cm ($\geq$ 30 GHz) only the nucleus shines brightly.

Infrared and millimetre observations have established the presence of a compact circumnuclear disk (Israel et al. 1990, 1991; Rydbeck et al. 1993; Hawarden et al. 1993; Sect. 5.2). At wavelengths shorter than 1 mm ($\geq$ 300 GHz), thermal emission from this compact circumnuclear disk becomes a new and important source of confusion (Cunningham et al. 1984; Hawarden et al. 1993). Although at the wavelengths and resolutions at which the nucleus itself can be seen, absolute flux-density determinations suffer from various calibration problems, it is clear that it is strongly time-variable (Sect. 5.6). The highly collimated nuclear radiojets likewise vary their structure and intensity with time (Jauncey et al. 1995; Tingay et al. 1998).

5.2. The circumnuclear disk

Analyzing CO measurements and infrared data from the literature, Israel et al. (1990; 1991) discovered a circumnuclear disk at the core of NGC 5128, with an estimated gas mass $10^7 M_\odot$. Its outer radius is 110-280 pc and it contains a central region of radius 40 pc, devoid of CO. Such a 100 pc-scale disk appears to be a common feature of active galaxies (*cf.* Maiolino & Rieke 1995). The CO gas in the disk has excitation temperatures of the order of 25 K and is significantly warmer than the CO gas in the dust band (T_{ex} = 10-15 K (Sect. 4.2). The kinematic signature of this rapidly rotating circumnuclear disk is evident in central CO profiles (Israel et al. 1991), as well as in major-axis position-velocity diagrams (*cf.* Fig. 2 of Quillen et al. 1992). The total dynamical mass within the disk area is estimated at about $10^9 M_\odot$, i.e. a hundred times higher than the molecular gas mass (Israel et al. 1991; Rydbeck et al. 1993). *Emission* from other molecular species in the circumnuclear disk, such as HCO^+, HCN, HNC and probably also C_3H_2, HNCO and H_2CO, has also been detected (Israel 1992).

Although the disk may have been revealed by its near-infrared extinction (Meadows & Allen 1992), it is the observations at

450μ and 800μm by Hawarden et al. (1993) that provided its first direct image. Its major axis is at position angle 140° - 145° (Hawarden et al. 1993; Rydbeck et al. 1993), quite different from that of the dust band, but perpendicular to the position angle of the jets (Sects. 2.4 and 5.4). The unresolved source seen in limited-resolution far-infrared (Joy et al. 1988) and mid-infared observations (Fig. 9) is due to thermal emission from this disk, as the flat-spectrum nonthermal nucleus is expected to contribute no more than about 25%-30% to the total observed emission at 100μm.

The disk appears to be larger in the J=1-0 transition than in the J = 2-1 transition (*cf.* Rydbeck et al. 1993). At submillimetre wavelengths it is larger again than in CO or at 100μm continuum. This suggests a temperature gradient across the disk, in addition to the density gradient postulated by Israel et al. (1990). Such a temperature gradient is to be expected if the excitation of the circumnuclear disk is caused primarily by winds and high-energy radiation from the power-law nucleus impinging on the cavity walls. The very red near-infrared colours, with their implicit suggestion of elevated dust temperatures in the inner region (Sect. 5.3) in addition to high extinction, as well as the compactness of [FeII] and H_2 emission from the centre (Israel et al. 1990; Meadows & Allen 1992) support this picture. Such near-infrared line emission is commonly interpreted as evidence either for shocks or for strong X-ray/UV irradiation, also required by X-ray observations (Feigelson et al. 1981; Turner et al. 1997; see Sect. 5.5). Mouri (1994) has suggested that the H_2 emission, with a temperature of about 1000 K, is excited by UV radiation from the nucleus, implying local densities in excess of 10^5 cm^3 (Sternberg & Dalgarno 1989). This is supported by the detection of X-ray line emission and absorption indicating the presence of variably ionized absorbing clouds vigorously interacting with the nuclear continuum radiation (Morini et al. 1989; Sugizaki et al. 1997; Turner et al. 1997).

Unpublished observations by P. van der Werf (private communication) show the outer radius of hot, vibrationally excited H_2 emission to be about 40 pc where it is rotating with 215 $km\ s^{-1}$ (Fig. 10). This implies a dynamical mass of $4.4 \times 10^8\ M_\odot$ within 40 pc, or an almost twentifold increase of mass per unit volume going from R = 150 pc to R = 40 pc. Assuming the outer limit of the extent of excited H_2 emission to mark the cavity radius (Koornneef & Israel 1996), it is doubtful whether the nucleus of NGC 5128 is powerful enough to provide the required excitation by radiation alone (Israel et al. 1990). Unless disk material extends much further inwards, it cannot control the collimation of the nuclear jets either, because this occurs on significantly smaller scales (see Clarke et al. 1992; Jones et al. 1996). Whether or not there is another, much smaller and thinner accretion disk of the sort proposed by e.g. Krolik & Lepp (1989), it should be emphasized that the agent collimating the jets must be closely, if possibly indirectly, connected with the circumnuclear disk discussed here in order to explain the excellent alignment between its rotation axis and the observed jet flow.

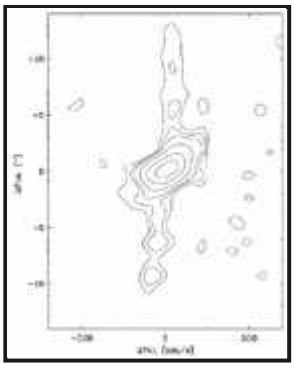

Figure 10. Velocity-position map of the distribution of excited molecular hydrogen at the inner edge of the circumnuclear disk. The bright central source indicates rapid rotation close to the nucleus. Courtesy P. van der Werf, University of Leiden.

5.3. Nuclear emission at infrared wavelengths

Optically, the core of NGC 5128 is completely obscured. Because dust extinction in the near-infrared is much less than at optical wavelengths (e.g. $A_K \approx 0.09 A_V$), the core has been frequently observed (Becklin et al. 1971; Kunkel & Bradt 1971; Grasdalen & Joyce 1976; Lépine, Braz & Epchtein 1984) as well as mapped (Harding, Jones & Rodgers 1981; Quillen, Graham & Frogel 1993; Adams, Adamson & Giles 1983; Giles 1986; Joy et al. 1991; Meadows & Allen 1992; Turner et al. 1992; Golombek, quoted in Schreier et al. 1996) in the 1-5μm wavelength range. Near-infrared images longwards of 2μm, usually

show a compact source close to the central position, but it is questionable whether this represents direct emission from the nucleus (see e.g. Antonucci & Barvainas 1990).

The relatively large-scale K-band maps by Quillen et al. (1993) and Adams et al. (1983) show a central 2.2μm peak embedded in an extended emission component in addition to several foreground stars. The extended emission is mostly due to the innermost stars of the elliptical galaxy, although there is also some emission from stars and HII regions in an inner dust lane of outer radius of 80" and projected thickness of 15" (Harding et al. 1981; Quillen et al. 1993; Adams et al. 1983; Meadows & Allen 1992). These K-band images show the "blossoming" of emission northeast of a dust absorption band, visible even at this wavelength, that extends across the nucleus. Below 2μm, the central feature is cometary in shape, points to the southwest in the same position angle as the X-ray/radio jet (Sect. 2.4) and is less compact than at longer wavelengths. The northeastern part of this feature corresponds to the UBVRI "hot spot" discovered by Kunkel & Bradt (who prematurely identified it with the nucleus). Joy et al. (1991) speculated that this cometary J/H-band "blue" source is the near-infrared counterpart of the X-ray/radio jet discussed in Sect. 2.4. However, its "blue" infrared colours and high degree of polarization are consistent with reflected light from a stellar or active nucleus in a clear line of sight (*cf.* Turner et al. 1992; Packham et al. 1996; Schreier et al. 1996), whereas the opening angle of the "blue" component is much wider than that of the radio/X-ray jets.

The position of peak emission moves to the southwest with increasing wavelength (*cf.* Schreier et al. 1996). The accuracy of positional measurements is insufficient to determine whether or not the K-band peak coincides with the nucleus (for the best position determinations see Giles 1986), but data tabulated by Schreier et al. (1996) suggest it is still somewhat off. Near-infrared polarimetry of the visually obscured centre of NGC 5128 has shown that, with increasing wavelength as well as with decreasing aperture, the position angle of the polarized vectors steadily increases from $PA \approx 120°$ to $PA = 145°$ (Bailey et al. 1986; Packham et al. (1996), i.e. from parallel to the dust band to parallel to the circumnuclear disk and perpendicular to the radio jet. At the "nuclear source", the intrinsic polarization is 17%. Schreier et al. (1996) further showed that this polarization peak coincides with a compact knot close to both the extinction and K-band emission peaks. The knot appears to be a heavily obscured interstellar cloud, scattering the optical and near-infrared radiation of the invisible nearby nucleus toward our line of sight. The absence of significant polarization at *millimetre* wavelengths led Packham et al. (1996) to reject Bailey et al.'s (1986) notion of an intrinsically highly polarized nucleus, emitting near-infrared synchrotron radiation and instead led them to conclude that the nucleus itself is obscured even at near-infrared wavelengths with $A_V = 16$ mag and that the "nuclear" polarization is produced by scattering and not by synchrotron emission or dichroic extinction.

Thus, the true nucleus is only fully revealed at wavelengths longer than 2.2μm, and the compact K-band source is mostly due to reflected light. Indeed, the extinction of the *nucleus itself* is variously estimated to be $15 \leq A_V \leq 60$, centering on $A_V = 25$-30 (see Lépine et al. 1984; Giles 1986; Turner et al. 1992; Meadows & Allen 1992, and references therein). As this is much higher than the extinction caused by the dust band (Sect. 4.4), the nucleus must be obscured primarily by the circumnuclear disk. Apart from the extinction problem, it is extremely difficult to determine reliable flux-densities, colours or even the very reality of weak unresolved K-band sources in galaxy centres, because of the practical difficulties in separating such sources from the central cusp of the surrounding galaxy (Simpson 1994; see also Fig. 8 by Turner et al. 1992).

The nucleus of NGC 5128 does appear as an infrared point source at 3.3 μm (Turner et al. 1992) and at 10μm (size $\leq$ 1" i.e. $\leq$ 16 pc; flux 1.4 Jy - P. van der Werf, private communication); it also is variable at least at 3μm (Lépine et al. 1984; Turner et al. 1992; see Sect. 5.6). Observations at longer infrared wavelengths so far have lacked the resolution to accurately separate the nucleus from the circumnuclear disk emission.

Infrared spectra centered on the nucleus show emission lines due to molecular hydrogen (H_2), Brackett- γ and [FeII] (Israel et al. 1990; Meadows & Allen 1992), but lack the noticeable CO-band absorption (characteristic for late-type stellar populations) which is seen off the nucleus where, in turn, the emission lines are absent (Meadows & Allen, 1992). The near-infrared colours of the central area, in contrast to those of the "blue feature" mentioned above, are extremely red, going from $J - H = 1.5$, $H - K = 0.9$ in a 2.5" aperture (Turner et al. 1992) to $J - H = 1.35$, $H - K = 1.75$ in a 1" aperture (Giles 1986). The very red colours are confined to a region within 12" from the nucleus (Giles 1986). They are far too red be caused by extinction. A rather similar situation has been found for NGC 3079 by Israel et al. 1998 who interpret such colours as due to a combination of extinction and emission from hot (1000 K) dust grains. Reddened synchrotron emission, also considered by Turner et al. (1992) appears to be ruled out by the work of Packham et al. (1996) discussed above.

5.4. The radio nucleus and nuclear jet

At the core of Centaurus A lies a compact radio nucleus for which (Kellerman, Zensus & Cohen (1997) have measured a size of 0.5 ± 0.1 milli-arcsec corresponding to linear dimensions of only 0.008 pc or 1700 AU). As there may be unresolved fine-scale structure even at this resolution, actual nuclear dimensions could be even smaller, the *lower limit* being about 10^{16} cm or 700 AU (Grindlay 1975; Mushotzky et al. 1978; Jourdain et al. 1993).

The nuclear source has a strongly inverted spectrum ($\alpha \approx 4$; Jones et al 1996). It is all but invisible below 5 GHz, but shows up in VLBI maps at 8.4 GHz with significantly time-variable flux-densities ranging over an order of magnitude (Preston et al. 1983; Meier et al. 1989; Jauncey et al. 1995; Jones et al. 1996; Tingay et al. 1998). Below about 20-30 GHz the radio emission from the nucleus probably suffers from both synchrotron self-absorption and free-free absorption in a circumnuclear ionized gas (Jones et al. 1996). Above the turnover frequency, the spectrum appears to remain flat (flux-density about 8-10 Jy up to at least 1000 GHz (*cf.* Kellerman et al. 1997).

Very high resolution (VLBI) radio measurements are needed to separate the extremely compact nucleus from its surroundings. Over some 65 milli-arcsec (projected linear distance 1 pc) a bright linear jet can be traced emanating from the nucleus at a position angle of 51° and with a width of a few milli-arcsec (Preston et al. 1983; Jones et al. 1996). The VLBI maps by Jones et al. (1996) and Tingay et al. (1998) show a weak counterjet to the bright northeastern nuclear jet. The jet components have very similar spectral indices $\alpha = -0.77$ and, like the nucleus, are variable in intensity (Meier et al. 1989). Monitoring the jet over several years, Tingay et al. (1998) found significant structural (c.q. intensity) changes of the knots in the jet (Fig. 11), implying internal evolution as well as a subluminal projected motion $v \approx 0.1c$ of the knots.

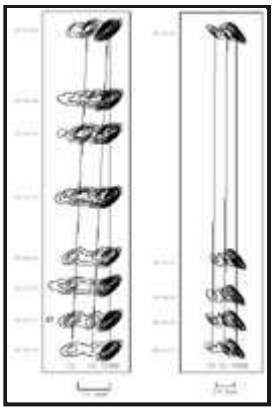

Figure 11. VLBI maps of the core and nuclear jet at 8.4 GHz over the period 1991-1996 identifying major components, and showing jet motion. From Tingay et al. (1998).

This *observed motion* may in fact represent slow patterns superposed on a significantly faster relativistic jet flow (Tingay et al. 1998). The large difference in jet and counterjet brightnesses can be explained by relativistic doppler beaming, enhancing the radiation of the jet approaching us. From the observed brightness ratio of 4-8, it appears that the northeastern jet is approaching and the southwestern jet receding at an angle of 50°-80° to the line of sight at moderately relativistic speeds $v \geq 0.45c$ (Jones et al. 1996; Tingay et al. 1998; see also Bao & Wiita 1997). The two brightest knots C1 and C2 separated recently from the nucleus, in 1983 and in 1989 respectively (Tingay et al. 1998).

There is still a significant gap in radio coverage of the nuclear region between aperture synthesis maps (5 GHz *resolution* 0.3": Clarke et al. 1992) and VLBI maps (8.4 GHz *coverage* $\approx$ 0.1": Jauncey et al. 1995; Tingay et al. 1998) so that a full description of the nuclear jets is still lacking. Since the nuclear jet velocities are much higher than those estimated for the inner jet (Sect. 2.4), significant deceleration must take place just at the missing size range so that any possibility of filling the observational gap should be pursued.

5.5. X- and γ-ray emission from the nuclear region

The hard X-ray/soft γ-ray emission is thought to arise from Compton up-scattering of lower energy photons by relativistic electrons; the photons may be supplied by the relativistic electrons themselves via the synchrotron self-Compton process, or by accretion heating. Major outbursts, correlated at X-ray and radio wavelengths, would then represent injection of fresh relativistic electrons, or re-acceleration of Compton-cooled electrons. They should decline on timescales determined by synchrotron loss rates, i.e., a few years. Faster variations probably reflect source expansions (Grindlay 1975; Mushotzky et al. 1978; Baity et al., 1981; Skibo et al. 1994; *cf.* Bond et al. 1996). Unlike the nucleus, at least the outer jets radiate primarily at soft X-ray energies (Feigelson et al. 1981; Turner et al. 1997)

The best available X-ray resolution, 6" provided by the ROSAT HRI, is insufficient to separate the nucleus and the nuclear jets, and even the innermost part of the inner jet. The energy distribution of the nucleus has been characterized by power-law spectra (Ubertini et al. 1993 Jourdain et al. 1993; Miyazaki et al. 1996; Sugizaki et al. 1997; Turner et al. 1997) with exponential cutoffs at 200-300 keV during periods of increased activity and 700 keV during quiescent periods (Kinzer et al. 1995). Centaurus A is difficult to detect above energies of 1 MeV (see Kinzer et al. 1995 and references therein) where the BL-Lac object MS1312-4221, 2° west of Centaurus A is also a potentially serious source of confusion (Fichtel et al. 1994; Kinzer et al. 1995; Thompson et al. 1995). In particular, detections in the 1-20 MeV range by von Ballmoos et al. (1987) were not confirmed by O'Neill et al. (1989), although the latter observed the nucleus in a more intense state. Likewise, an early detection at very high energies (Grindlay et al. 1975) could not be repeated (Carramiñana et al. 1990; *cf.* Allen et al. 1993). However, observations with COMPTEL have now provided good detections in the 1-30 MeV range (Steinle et al. 1998), which together with a 200 MeV EGRET detection (Thompson et al. 1995) allow the spectrum to be fitted with sets of broken power laws, with spectral indices steepening from α = - 1.7 to -2.0 to -2.6 for the low ($L_\gamma = 3 \times 10^{42}$ erg s^{-1}) intensity state and from α = - 1.7 to -2.3 to -3.3 for the intermediate ($L_\gamma = 5 \times 10^{42}$ erg s^{-1}) intensity state.

Turner et al. (1997) concluded that nuclear emission dominates the X-ray flux above 2 keV and estimated that 40% of the source suffers extinction by a column $N_H = 4 \times 10^{23}$ cm^{-2}, 59% by a column $N_H = 1 \times 10^{23}$ cm^{-2} and the remaining 1% by a column two orders of magnitude less. It is tempting to ascribe the first fraction to the nucleus itself, and the second to the nuclear jets, but there is no real evidence supporting this speculation. It is clear, in any case, that both components are obscured by the circumnuclear disk discussed in Sect. 5.2 whose estimated parameters fit the X-ray observations rather well. X-ray K-edge absorption and fluorescent emission from Fe at 6.4 keV (Mushotzky et al. 1978; Wang et al. 1986; Morini et al. 1989), but also Mg, Si and S (Sugizaki et al. 1997) can be explained by irradiation and reprocessing of clouds in the circumnuclear disk by the nuclear X-ray source (*cf.* Morini et al. 1989; Turner et al. 1997) and thus provide independent evidence for the fierce interaction of the nucleus with the inner parts of the circumnuclear disk.

5.6. Variability of the nucleus

Both the nucleus and the jet structures within at least 0.1' are variable. As they do not seem to vary in tandem (Tingay et al. 1998) and have different spectra, accurate determinations of the spectral index and its time variation are extremely difficult to make especially with relatively large single-dish beams. At 1.4 GHz, considerable variability is seen on timescales of a hundred days or longer (Romero, Benaglia & Combi 1997). As the amplitude of variation is large, and the nucleus is strongly (self)absorbed at this frequency (Sect. 5.4), it cannot reflect activity in the nucleus itself. Instead, shocks interacting with density inhomogeneities in the inner jet appear responsible. Well-established variability at higher frequencies is harder to interpret. Large-beam monitoring by Botti & Abraham (1993) has yielded large flux (22 GHz: 16-32 Jy; 43 GHz: 6-20 Jy) and spectral index variations ($\Delta \alpha$ = 2), while Kellerman et al. (1997) noted a 60% drop in 43 GHz intensity over only 3 months Qualitatively, this may reflect expansion of the nuclear source and jets, initially opaque and then becoming (partially) optically thin. However, the large beams used include significant non-nuclear emission from the nuclear and inner jets, confusing the issue.

Nevertheless, the radio variability appears to be correlated with that at hard X-ray wavelengths (Botti & Abraham 1993; Jourdain et al. 1993; Turner et al. 1997) which must be associated with the nucleus. The 3-12 keV light curve presented by Turner et al. (1997) for a 26-year period (based largely on the Vela 5B light-curve from Terrell 1986, and sparsely sampled after 1980) shows major outbursts in 1972-1976 and in 1979 (see also Feigelson et al. 1981; Baity et al. 1981; Gehrels et al. 1984; Bond et al. 1996) when the observed X-ray fluxes increased by an order of magnitude. These outbursts were separated by a low-intensity state with fluctuations by a factor of two. At millimetre wavelengths, likewise sampling nuclear behaviour, the 1972-1976 maximum is evident in the 90 GHz measurements by Kellermann (1974) and Beall et al. (1978). The 90-800 GHz measurements by Cunningham et al. (1984; see also Hwarden et al. 1993) show that the outburst starting in 1979 was still going on in 1981, which is also confirmed at 100 keV (Gehrels et al. 1984; Jourdain et al. 1993). A poorly covered outburst occurred in 1985 (Jourdain et al. 1993; Bond et al. 1996; Turner et al. 1997); this outburst may be associated with the expulsion of radio knot C1 (Tingay et al. 1998). The near-infrared 3.5μm variability noted by Lépine et al. (1984) and Turner et al. (1992) follows a pattern similar to that of the radio and X-ray emission (low in in 1971 and 1987, high in 1975 and 1981) suggesting that the emission at this wavelength arises from a similar or identical mechanism.

The observed 0.1-2 keV luminosity of the nuclear region increased by a factor of two between 1990 and mid-1993. A probably related rise was seen in the 43 GHz radio flux occurring at the end of 1992 lasting into early 1993 (Abraham 1996). However, no flux increase was seen at hard X-ray energies (Turner et al. 1997; Bond et al. 1996) whereas 100/230 GHz monitoring by Tornikoski et al. (1996) reveals only modest ($\leq$ 50%) flux increases over relatively short times in 1992/1993 and 1994/1995. As both hard X-rays and millimetre wave frequencies sample the nucleus rather than the jets, this suggests that the soft X-ray/43 GHz increase is related to the jet expansion observed by Tingay et al. (1998) and not to nuclear activity.

The hard X-ray flares of July/October 1991 (Jourdain et al. 1993; Bond et al. 1996) were unfortunately not covered by the millimetre monitoring programme. The October 1991 flare is evident, however, in γ-ray observations by Kinzer et al. (1995); see also γ-ray fluxes listed by Steinle et al. (1998) for the period 1991-1995, and their graph of the hard X-ray variability over the same period showing significant activity in mid-1994. Minor X-ray flares in the low-intensity state have doubling times of about two days and last for one or two weeks; they appear to occur several times a year (Terrell 1986; Beall et al. 1987; Jourdain et al. 1993; Turner et al. 1997) and involve energy transfers of order 10^{42} erg s^{-1} (Terrell 1986; Bond et al. 1996). The nucleus seems to have been in the quiescent, low-intensity state for most of the time since 1989, as also indicated by the 8.4 GHz VLBI core monitoring by Tingay et al. (1998). In addition to these variations, there is at least at X-ray and soft γ-ray wavelengths a considerable small-amplitude (10-20%) variation at timescales of minutes and hours (Morini et al. 1989; Kinzer et al. 1995; Miyazaki et al. 1996; Turner et al. 1997, but see also Jourdain et al. 1993). Very fast flux variations reported by Wang et al. (1986) have not been confirmed and are now generally doubted.

6. KINEMATICS AND DYNAMICS

6.1. Kinematical studies

Over the last two decades, several major kinematical studies have been carried out of both the ellipsoidal and the disk component of NC 5128. The kinematics of the ellipsoidal component have been traced by studies of the motions of stars (Wilkinson et al. 1986), globular clusters (Hesser, Harris & Hesser 1986; Harris, Harris & Hesser 1988) and planetary nebulae (Hui et al. 1985).

Stellar motions were fully mapped by Wilkinson et al. (1986) over 100" and supplemented by major axis data out to 400" (6.6 kpc). The ellipsoidal stellar component is rotating rather slowly at velocities not surpassing 40 $km\ s^{-1}$ in the line of sight around an axis at position angle 135°, i.e. rotating only roughly perpendicular to the dust lane. The velocity dispersions range from 95 to 150 $km\ s^{-1}$. The planetary nebula system, studied by Hui et al. (1995) out to 20', has a similar mean velocity dispersion of 110 $km\ s^{-1}$. Major axis rotation increases to 100 $km\ s^{-1}$ at 7 kpc and after that remains constant to at least 22 kpc. Minor axis rotation is less than 50 $km\ s^{-1}$ out to the last observed radius of 10 kpc. The projected rotation axis is at position angle 165°, i.e. displaced from the photometric minor axis (and disk orientation) by about 40°; the line of zero rotation is not orthogonal to the line of maximum rotation. Such observations suggest that NGC 5128 has a triaxial potential. The kinematics of the globular cluster system again appear to be similar to those of the spheroidal stellar system (Hesser et al. 1986; Harris et al. 1988). In particular, the metal-rich globular clusters rotate very much like the planetary nebulae, whereas the metal-poor clusters appear to lack significant rotation (Hui et al. 1995).

The rich gas content of the dust lane (Sects. 4.1 and 4.2) has allowed detailed kinematical studies of the disk component to be performed in lines of ionized hydrogen (Bland, Taylor & Atherton 1987), neutral atomic hydrogen (van Gorkom et al. 1990; Schiminovich et al. 1994) and CO (Eckart et al. 1990a; Quillen et al. 1992; Wild et al. 1997). Optical and radio observations (Graham 1979; van Gorkom et al. 1990; Quillen et al. 1992) show the disk to be in rapid rotation with a rotation gradient of about 150 $km\ s^{-1}$ kpc^{-1} close to the nucleus, in sharp contrast to the rather modest rotation of the elliptical component. Graham (1979) estimated the plane of rotation to be tilted by 73° with respect to the plane of the sky. Bland et al. (1987) mapped the ionized hydrogen gas at arcsec resolution over 7' × 5', with a moderate velocity resolution of 36 $km\ s^{-1}$ similar to that obtained by Wilkinson et al. (1986); the neutral hydrogen observations have comparable velocity resolutions. Although the CO observations have high velocity resolutions of about 1 $km\ s^{-1}$, that advantage is largely undone by their spatial resolution of 20"-40" causing significant beam-smearing which can only be partially undone by modelling.

The limited resolutions of the HI and CO data allow only relatively simple modelling of circular orbits in warped disks approximated by sets of variously tilted rings. Virtually all attempts to dynamically model the observed kinematics of the disk therefore rely largely or completely on the optical observations by Bland et al. (1987). Assuming circular motion consistent with an $r^{1/4}$ law mass distribution, Nicholson, Bland-Hawthorn & Taylor (1992) confirmed Graham's (1979) conclusion that the gas and dust are in a highly inclined rotating disk, with an amplitude V_{rot} = 250 $km\ s^{-1}$ at R = 2.0 kpc and a rotation gradient similar to the one derived by Graham (1979), eastern edge approaching. Projected onto the sky, the HII regions are confined to an envelope similar tothe form of a hysteresis loop, characteristic of a warped disk rather than a ring. They convincingly showed that the kinematical data can be represented by a class of models involving a thin warped disk geometry with a spatially averaged optical depth sufficiently low to allow emission from all positions of the disk to be seen. Double-peaked velocity profiles mark folds in the warped disk seen in projection. Quillen et al. (1992; 1993) confirmed that such an interpretation also applies to the dusty molecular disk.

6.2. Dynamical models

Kinematical information is restricted to the distribution on the sky of radial velocities only. The large number of free parameters in combination with observational limitations such as finite resolution and extinction, renders the outcome of dynamical modelling very sensitive to initial assumptions (*cf.* Kormendy & Djorgovski 1989). It is therefore not surprising that the general agreement on kinematical (tilted ring) models describing the motion of the disk component is not matched by a similar convergence on a unique dynamical model. For a review of the methods and problems of determining structure and dynamics of elliptical galaxies in general the reader is referred to De Zeeuw & Franx (1991).

Wilkinson et al. (1986) found a ratio of maximum rotational velocity to peak nuclear velocity dispersion characteristic of a rotationally supported oblate system seen almost edge-on (Davies et al. 1983). Assuming the radio jet to mark the long axis, an effectively stationary rotating nearly oblate triaxial model with axis ratios 1:0.98:0.55 provided their best fit; our line of sight is then 30°-40°-40 from the plane defined by the two long axes. Dropping the requirement of identical jet direction and stellar symmetry axis, they also found a satisfactory fit to an effectively stationary prolate spheroidal model. Following earlier work by Tubbs (1980), a prolate model with clouds moving in circular orbits in a warped disk was favoured by Quillen et al. (1992) on the basis of their CO observations and the ionized gas kinematics determined by Bland et al. (1987). Quillen et al. (1993) presented a revised version of this model to reproduce the morphology of their near-infrared maps.

Assuming the planetary nebulae to form a relaxed system (implying a triaxial potential), a stationary galaxy figure, and the gas disk to be in the preferred plane defined by the long axis, Hui et al. (1995) derived a model with axial ratios of 1:0.92:0.79 where the short axis lies in the plane of the sky, and the intermediate axis is along the line of sight. Mathieu, Dejonghe & Hui (1996) used the planetary nebula system to construct triaxial models, assuming a spherical potential obtained by inverting the major axis photometry. Failing to obtain satisfactory fits with constant M/L ratios, they concluded to a significant presence of dark matter, causing a significant increase of the mass-to-light ratio with radius. They consider the kinematics and photometry of NGC 5128 to be well described by two kinematically distinct subsystems supporting the merger hypothesis. On the whole, there is substantial agreement that the inner parts of NGC 5128 have a roughly constant mass-to-light ratio $M / L_B \approx 4$ increasing with radius to the extent that the *global* ratio of NGC 5128 is $M / L_B = 10$ (Hesser et al. 1984; van Gorkom et al. 1990; Hui et al. 1995; Mathieu et al. 1996). The total mass of the galaxy is $M = 4 \pm 1 \times 10^{11}$ M$_\odot$, with typically half of it due to dark matter (Mathieu et al. 1996). The galaxy mass is thus between 2% and 10% of the NGC 5128 / NGC 5236 group mass.

Interpreting the dust band as a precessing warped structure, Nicholson et al. (1992) ruled out prolate models and concluded that its geometry is consistent with a near-polar gas disk in an oblate, almost spherical triaxial potential with its short axis likewise in the plane of the sky. In their models, the dust band is separated into an inner detached disk (r <1.7 kpc) and an outer extended annulus (1.7 kpc < r < 6.8 kpc). Sparke (1996) showed that, at least qualitatively, such models can explain not only the the observed disk features but also the broken HI ring observed by Schiminovich et al. (1994). An important factor is the variation in oblateness of the galaxy, which is taken to be nearly spherical at small radii and more flattened farther out. Sparke's (1986) model resembles that of Wilkinson et al. (1986) but is in contradiction to that of Hui et al. (1995). The discrepancy may be resolved if, in fact, the planetary nebulae do not represent a relaxed and well-mixed system (Sparke 1996).

Of particular interest is the shell system referred to in Sect. 4.1 and shown in Figs. 6 and 7. Malin et al. (1983) interpreted the shells as the signature of the collision between a dynamically cold system and a rigid potential well (Quinn, 1984; Hernquist & Quinn 1988, 1989) under the condition that the infalling system had a mass significantly less than that of the elliptical galaxy. The shells arise from phase-wrapping of the disk after it has been disrupted by the tidal field of the massive elliptical galaxy. In fact, this work, as well as that by Tubbs (1980) served to underpin the galactic-encounter interpretation of NGC 5128 first suggested by Baade & Minkowski (1954) and revived by Graham (1979). Malin et al. (1983) suggested that a late-type galaxy of mass a few times 10^{10} $M_\odot$, similar to e.g. M 33, merged with NGC 5128 a few hundred million years ago. Specific, more detailed merger scenarios were presented by Tubbs (1980) and Quillen et al. (1993).

6.3. Evolutionary timescale

If the gas dust disk would define a preferred plane in a triaxial system, its rotation should be retrograde with respect to the tumbling motion of the stellar ellipsoid (van Albada, Kotanyi & Schwarzschild 1982). However, Wilkinson et al. (1986) found that the disk has in fact prograde rotation, and suggested the warped disk to be due to incomplete settling of material into a symmetry plane of the potential. This is consistent with the conclusion by van Dokkum & Franx (1995) that dust disks in early-type galaxies, with a radius exceeding 250 pc, are generally not settled. The disk would thus be a transient phenomenon, unless it were stabilized by self-gravity (Nicholson et al. 1992; see also Sparke 1996).

A stable disk is required if the merger and dust band formation occurred some 10^9 years ago (Graham 1979; Nicholson et al. 1992). Quillen et al.'s (1992; 1993) "short" timescales of 1-2 × 10^8 years were criticized by Sparke (1996) who estimated three quarters of a gigayear as the time elapsed since capture of a companion galaxy from a polar orbit. The presence of an intermediate age stellar population in the halo of NGC 5128 prompted Soria et al. (1996) to suggest an even longer timescale of several gigayear, while intermediate scales of 2-8 × 10^8 years (and incomplete settling) have been suggested by Tubbs (1980) and Malin et al. (1983). All these timescales are, however, much longer than the age of the current burst of star formation in the disk which is typically a few times 10^7 years (van den Bergh 1976; Dufour et al. 1979)

7. THE NUCLEAR ABSORPTION SPECTRUM

HI line absorption against the centre of Cen A over the velocity range of 500-600 $km\ s^{-1}$ was first recognized in single-dish observations by Roberts (1970) and Whiteoak & Gardner (1971; 1976b). It was studied at high spatial (2.6" × 11") and moderate velocity (6 $km\ s^{-1}$) resolutions by Van der Hulst, Golisch & Haschick (1983). Subsequently, centimetre wavelength absorption by various molecular species (OH, H_2CO, C_3H_2, NH_3) was observed by Gardner & Whiteoak 1976a, b; 1979; Seaquist & Bell 1986; 1988; 1990). The HI observations by van der Hulst et al. (1983) show the inner jets (20" and 30" northeast of the nucleus) as well as the nuclear source in absorption. The inner jets are also seen in H_2CO absorption (Seaquist & Bell 1990), while H_2CO absorption is likewise found in the direction of the dust band, 4' southeast from the nucleus (Gardner & Whiteoak 1976b).

The flat and strong nuclear continuum spectrum at millimetre wavelengths (Sect. 5.4) provides the opportunity to extend absorption studies to wavelengths where molecular line transitions are most abundant. High velocity resolution ($\Delta V \leq 2.6\ km\ s^{-1}$) absorption spectra of the lower transitions of ^{12}CO and ^{13}CO were obtained by Israel et al. (1990; 1991) and Eckart et al. (1990b). Various other molecular species, such as HCO^+, $H^{13}CO^+$, HCN, HNC, CS, C_2H, CN, C_3H_2 and H_2CO have likewise been detected in absorption (Eckart et al. 1990b; Israel et al. 1991; Wiklind & Combes 1997; Israel et al. unpublished). Centaurus A is unique in this sense: as of yet, no other active galactic nucleus is known to exhibit absorption by a molecular disk (Drinkwater, Combes & Wiklind 1996).

Below 10 GHz, emission from the inner and nuclear jet dominates the continuum, whereas above 30 GHz the continuum emission arises mostly or wholly from the nucleus. Thus, centimetre-wavelength single-dish measurements sample sightlines as far as 500 pc away from the nucleus while aperture synthesis observations, after elimination of the inner jet contribution, preferentially sample sightlines missing the nucleus itself by about 1.5 parsec, i.e. 200 times the diameter of the nuclear source. Only at (sub)millimetre wavelengths does the absorption sample a narrow line of sight (0.5 milliarcsec) directly to the nucleus.

A typical molecular line spectrum of the Centaurus A nucleus consists of a relatively strong emission line arising from the molecular disk (Sect. 4) as well as weaker and broader emission representing the circumnuclear disk (Sect. 4.2) superposed on the nuclear continuum (*cf.* Fig. 1 in Israel, 1992). As absorption occurs over a significant fraction of the total emission line spectrum, the intrinsic shape of the latter is hard to determine but of crucial importance in determining the pure absorption spectrum.

The absorption spectra show numerous peaks at various velocities (Fig. 12), relatively strong between 540 $km\ s^{-1} \leq V_{Hel} \leq$ 555 $km\ s^{-1}$, i.e. within 10 $km\ s^{-1}$ from the systemic velocity. It is not clear which of these lines, if any, marks the systemic velocity. There are at least five (blended) components in this velocity range but only two of these have discernible HI counterparts in VLA spectra (van der Hulst et al. 1983; J.M. van der Hulst, private communication). As these two HI features are also seen against the inner jets at 30" (500 pc) above the circumnuclear disk, they originate most likely in the more distant molecular disk associated with the dust band structure (*cf.* van der Hulst et al. 1983). This is consistent with the apparent low excitation of the corresponding molecular absorption lines, which suggest the material to be located at considerable distance to the nucleus (Gardner & Whiteoak 1979; Seaquist & Bell 1990; Eckart et al. 1990b). The velocity range is consistent with the velocity dispersion in the molecular disk (Quillen et al. 1992).

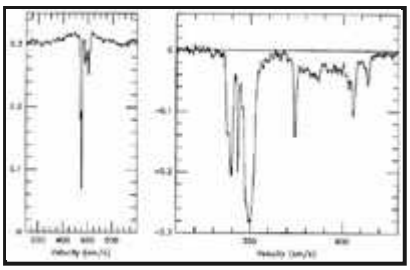

Figure 12. Nuclear absorption spectrum in HCO^+. Left: low velocity resolution (4.7 $km\ s^{-1}$) spectrum showing continuum, molecular line emission from circumnuclear disk and dark band, and molecular line absorption covering large velocity range. Right: high velocity resolution (0.3 $km\ s^{-1}$) spectrum showing several narrow absorption lines and "forest" of redshifted lines. Horizontal scale is V_{LRS}, vertical scale is antenna temperature (corresponding to 0.75 × main-beam brightness temperature). From Israel et al. 1991, and unpublished data.

Of particular interest is a second absorption line system, extending from V_{Hel} = 560 $km\ s^{-1}$. It is seen only against the nuclear source, and not against the inner jets (disregarding the marginal H_2CO feature seen by Seaquist & Bell 1990). This high-velocity, redshifted absorption system takes the shape of continous molecular absorption with a few individual peaks of relatively low optical depth (Israel et al. 1991; Wiklind & Combes 1997). The redshifted absorption system is also prominent in HI (Gardner & Whiteoak 1976b; van der Hulst et al. 1983). With respect to e.g. HCO^+, the HI absorption is relatively strong at 560 $km\ s^{-1} \leq V_{Hel} \leq$ 600 $km\ s^{-1}$, and weak at higher velocities. This redshifted system is generally interpreted as due tc infalling clouds (Gardner & Whiteoak 1976b; van der Hulst et al. 1983; Seaquist & Bell 1990; Israel et al. 1991). It implies accretion rates sufficiently high to explain the overall radio luminosity of Centaurus A (van Gorkom et al. 1989). As the absorption optical depth ratios of the various species appear to be a function of (infall) velocity, this opens the interesting possibility of modelling the processing of material falling into the nucleus of Centaurus A. As the optical depths and consequently signal-to-noise ratios are low, this is not an easy task.

At velocities 500 $km\ s^{-1} \leq V_{Hel} \leq$ 540 $km\ s^{-1}$ there is a hint of a very low optical depth blueshifted HCO^+ absorption wing (*cf.* Israel 1992; Wiklind & Combes 1997). Its nature is not clear, and it is not seen in HI (J.M. van der Hulst, private communication). High resolution OH maser absorption spectra against the nuclear source in the four transitions at 18 cm wavelength show exactly conjugate behaviour at all velocities in the satellite lines: the sum of the two transitions is zero (van Langevelde et al. 1995). This effect is caused by the competition of the two transitions for the same pumping photons and allows a direct determination of the OH column density $N(OH) \approx 6 \times 10^{15} cm^{-2}$.

8. Concluding summary

NGC 5128 is a massive elliptical galaxy at the heart of a moderately rich group of galaxies (Sect. 1.4); basic data are summarized in Table 3. Although most of its properties are fairly normal for a luminous triaxial elliptical galaxy, it is remarkable in two aspects: it hosts a very large radio source (Sect. 2) and its inner parts harbour a relatively massive disk of dust, gas and young stars (Sect. 4). Both have been proposed as the consequence of past merger activity. The location of the galaxy amidst several dwarf galaxies lends plausibility to such a suggestion. Indeed, although no *direct* evidence of a merger has been found, the appearance of the galaxy and in particular the properties of its embedded disk, such as gas mass, kinematics, warp and polar orientation along the photometric minor axis (*cf.* Bertola et al. 1988) as well as the bimodality of its globular cluster system (Zepf & Ashman 1993; Perelmuter 1995), the existence of luminous optical and and HI shells as well as the outcome of various dynamical models and scenarios (Sect. 6.2) all provide strong indirect evidence that at least one major merger event occurred some 10^8-10^9 years ago. The gas mass of the dusty disk, a few times $10^9 M_\odot$, point at capture of a fairly

sized late-type spiral galaxy rather than a small irregular. The shell structures in particular suggest that NGC 5128 experienced more than just one merger (Weil & Hernquist 1996).

The radio source Centaurus A, associated with NGC 5128, is a very near example of a large class of radio galaxies of moderate luminosity known as FR-I galaxies (Fanaroff & Riley 1974). Radio sources of this class are generally presumed to have moderately active nuclei with relativistic outflows on a subparsec scale not aligned with our line of sight. The observations of Centaurus A at radio and X-ray / γ ray wavelengths are consistent with this interpretation. NGC 5128 contains a very compact nucleus of size 1200 ± 500 A.U. from which subluminal relativistic jets emanate (sect. 5.4) that become subrelativistic within 1.5 pc. The jets appear to propagate at a large angle to our line of sight. The nucleus itself is strongly obscured by a small (radius $\approx$ 150 pc) circumnuclear disk (Sect. 5.2) and is quite variable at radio and X-ray wavelengths (Sect. 5.6). The polarization of the central region, the ionization of the optical filaments and the apparent similarity of the high-energy spectrum (but not the luminosity) of Centaurus A (in particular at γ-ray energies) to that of blazars and quasars such as 3C273, have been used to argue that the galaxy indeed harbours a misaligned BL Lac/blazar nucleus (Bailey et al. 1986; Morganti et al. 1991; Dermer & Schlickeiser 1993; Kinzer et al. 1995; see also Steinle et al. 1998, and references therein). The substantially lower luminosity of Centaurus A is then explained by our viewing the galaxy from the side, and not down the jet axis. However, some caution to this conclusion has been expressed by Antonucci & Barvainis (1990) and Kellerman et al. (1997).

Table 3. NGC 5128 Basic Data

	Value	Units	Reference
$\alpha(1950)_0$	13:22:31.6 ± 0.2		Giles 1986
$\delta(1950)_0$	-42:45:30.3 ± 0.4		Giles 1986
Galactic Longitude l	309.5	degrees	
Galactic Latitude b	+19.4	degrees	
Systemic Velocity V_{Hel}	543 ± 2	$km\ s^{-1}$	Table 1
Galaxy Size D_{25}	18 × 14	arcmin	RC2
Radio Source Size	8 × 4	degrees	Section 2.1
Distance	3.4 ± 0.15	Mpc	Section 1.2
Apparent Magnitude B	7.96	mag	RC2
Colour $(B - V)_T$	0.98	mag	RC2
Foreground Reddening $E(B - V)$	0.11	mag	Section 3.4
Total Galaxy Mass	$4 \pm 1 \times 10^{11}$	$M_\odot$	Mathieu et al. 1996
Total HI Mass	$8.3 \pm 2.5 \times 10^{8}$	$M_\odot$	Section 4.2
Gas Mass Dusty Disk	$1.3 \pm 0.4 \times 10^{9}$	$M_\odot$	Section 4.2
Gas Mass Circumnuclear Disk	$1.1 \pm 0.3 \times 10^{7}$	$M_\odot$	Section 5.2
Linear Sizes:			
Outer Radio Lobe	250	kpc	Section 2.1
Middle Radio Lobe	30	kpc	Section 2.2
Inner Radio Lobe	5	kpc	Section 2.3
Inner Radio Jet	1.35	kpc	Section 2.3
Relativistic Nuclear Jet	1.65	pc	Jones et al. 1996
Radio Core	0.008	pc	Kellerman et al. 1997
Radius Dusty Disk	7	kpc	Section 4.1
Radius Circumnuclear Disk	150(-40, +130)	pc	Section 5.2

Nuclear activity must have been going on for a considerable amount of time, given the size of the outer radio lobes. The bulk speeds of 5000 *km* s^{-1} estimated for the inner jets (Sect. 2.4) and the outer radius of 250 kpc of the giant lobes of radio emission suggest *a lower limit* of 50 million years. As the inner jets appear to dissolve into plumes ("inner lobes") at about 5 kpc from the nucleus (Sect. 2.3), and as the position angle of the outer radio features is much different from that of the inner features, it is reasonable to conclude that significant deceleration occurs over most of the radio source, leading to a substantially higher age. Indeed, the age of the inner lobes alone was already estimated at 6×10^8 years (Slee et al. 1983), although this may be too high. The jets appear to lose much of their energy within a few parsec from the nucleus, presumably by interaction with ambient material. The peculiar radio brightness evolution of component C1 in the nuclear jet may provide a clue to this process (Tingay et al. 1998) underscoring the need for further VLBI monitoring of Centaurus A, as well as the desirability of filling the resolution gap in the 0.1-0.3" range. The inner jets dissolve in the more extended inner lobe plumes, which exhibit a profound clockwise bending (decreasing position angle). Again, ambient material and its movement in the galaxy, may explain the observed morphology (see e.g. Sparke 1982; Gopal-Krishna & Saripalli 1984; Heckman et al. 1985), but hard evidence is lacking. Moreover, this is unlikely to also explain the similarly profound clockwise bending of the giant outer lobes, well outside the optical galaxy. Noting a continuous decrease of position angle (i.e. clockwise bending) of various features at increasing distance to the nucleus, Haynes et al. (1983) have proposed that the central collimating source precesses at a rate of the order of 10^{-5} degrees per year. The discovery of a circumnuclear disk perpendicular to the nuclear and inner jet, yet inclined to the minor axis of the elliptical galaxy, supports the idea of precession. If the rate of procession is correctly estimated, the structure of the radio source should exhibit the effect of several precessional periods. It would be interesting to see whether the run of position angles with radius can indeed be modelled by such a precession of the collimating agent. Alternatively, a combination of precession and ambient gas dynamics may be required, while the structure of the outer lobes, in addition, may be influenced by tumbling and orbital motion of the galaxy as a whole (Burns et al. 1983).

The putative age of the merger (Sect. 6.3) suggests a link to the origin of the radio source. Although the presence of an active nuclear source predating a merger cannot be excluded, it is tempting to associate its origin with the accumulation of matter in the centre caused by transfer of angular momentum through viscous damping after such an event. An intriguing indication that the origin of the radio source is connected to merger activity is provided by a morphological argument. The bended appearance of the giant radio lobes (Fig. 4) is very similar to that of the tilted rings forming the dust band (*cf.* Fig. 11b in Nicholson et al. 1992) rotated by 90°. For instance, the position angle of 0° characterizing the outer radio contours corresponds to the position angle of 90° of the outer rings. Because the dynamical time scale of the outer rings is much longer than that of the more strongly tilted inner rings, their *present* position angle should more closely resemble the *original* orientation of the inner disk structure at the time that the matter now forming the outer lobes was ejected. As the dust disk originated in a merger event, and the morphology of the radio lobes appear to follow its subsequent evolution, it seems likely that the activity creating these lobes is also a consequence of the merger event.

If the nuclear source is in fact a black hole, its estimated bolometric luminosity (half of it at high energies) of about 10^{43} erg s^{-1} implies a *lower limit* to the black hole mass of about 5×10^4 $M_\odot$ whereas the total luminosity of the radio source suggests a mass $\geq 10^7$ $M_\odot$ (Terrell 1986 and references therein; Kinzer et al. 1995). As the dynamical mass within 40 pc is about 4×10^8 $M_\odot$, and there is no obvious sign of Keplerian rotation (see Fig. 10), its *upper limit* must be a few times 10^7 $M_\odot$. Although the high obscuration of the centre of NGC 5128 and the lack of H_2O masers (Braatz et al. 1996) precludes, at the moment, a more accurate mass determination, the actual mass of the putative black hole nevertheless is fairly well-constrained and is comparable to that of the circumnuclear disk (Sect. 5.2). This mass is not very high and infalling molecular clouds, especially dense cores, may penetrate deeply before being tidally disrupted. The variability of the nucleus may represent the accretion of individual stellar or cloud remnants onto the black hole triggering renewed jet activity (Sect. 5.4 through 5.6) and fueling the radio source. Details of these processes are not clear yet, but careful and frequent monitoring of Centaurus A at radio, X-ray and γ-ray wavelengths may provide important information. For instance, how does the nucleus drive the nuclear jets, and how are the relativistic nuclear jets transformed into the nonrelativistic inner jets? The circumnuclear disk (Sect. 5.2) does not seem capable of controlling the collimation of the nuclear jets, but its orientation exactly perpendicular to these jets, suggests that it is somehow connected with the collimating agent. Comparison of Centaurus A features with very-high resolution observations (HST, VLBA) of other active elliptical galaxies suffering less nuclear extinction, such as the ten times more distant NGC 4261 (e.g. Jones & Wehrle 1997, and references therein) may prove particularly fruitful.

Acknowledgement. It is a pleasure to thank David Malin, Do Kester, Norbert Junkes, Thijs van der Hulst, Stéphanie Côté, Steven Tingay, Jack Burns and Paul van der Werf for kindly supplying the illustrations in this review. I also would like to thank

Paul van der Werf, Hans Bloemen, George Miley and in particular Tim de Zeeuw for critical comments on an earlier version of this work. The burden of literature searches was greatly relieved by the use of the NASA Astrophysics Data System (ADS) Astronomy Abstract Service.

REFERENCES

1. Abraham Z., 1996, in: "Extragalactic Radio Sources", IAU Symposium 175, Eds. R. Ekers, C. Fanti, L. Padrielli, (Dordrecht: Kluwer), p. 25
2. Adams D.J., Adamson A.J., Giles A.B., 1983 MNRAS 202, 241
3. Allen L.R., Hanbury Brown R., Palmer H.P., 1963 MNRAS 125, 57
4. Allen W.H., Bond I.A., Budding E., et al. 1993 ApJ 405, 554
5. Alonso M.V., Minniti D., 1997 ApJS 109, 397
6. Antonucci R., Barvainas R., 1990 ApJL 363, L17
7. Arp H., 1994 A&A 288, 738
8. Baade W., Minkowski R., 1954 ApJ 119, 215
9. Bailey J., Sparks W.B., Hough J.H., Axon D.J., 1986 Nature 322, 150
10. Baity W.A., Rothschild R.E., Lingenfelter R.E., et al., 1998 ApJ 244, 429
11. Bao G., Wiita P.J., 1997 ApJ 485, 136
12. Beall J.H., Rose W.K., Graf W., et al. 1978 ApJ 219, 836
13. Becklin E.E., Frogel J.A., Kleinmann D.E., et al., 1971 ApJL 170, L15
14. Bell M.B., Seaquist E.R., 1988 ApJL 329, L17
15. Bertola F., Galletta G., Kotanyi C., Zeilinger W.W., 1988 MNRAS 234, 733
16. Bland J., Taylor K., Atherton P.D., 1987 MNRAS 228, 595
17. Bolton J.G., 1948 Nature 162, 141
18. Bolton J.G., Stanley G.J., Slee O.B., 1949 Nature 164, 101
19. Bond I.A., Ballet J., Denis M., et al. 1996 A&A 307, 708
20. Botti L.C.L, Abraham Z., 1993 MNRAS 264, 807
21. Braatz J.A., Wilson A.S., Henkel C., 1996 ApJS 106, 51
22. Branch D., Romanishin W., Baron E., 1996 ApJ 465, 73
23. Branch D., Fisher A., Baron E., Nugent P., 1996 ApJL 470, L7
24. Brodie J., Königl A., Bowyer S., 1983 ApJ 272, 154
25. Brodie J., Bowyer S., 1985 ApJ 292, 447
26. Burns J.O., Feigelson E.D., Schreier E.J., 1983 ApJ 273, 128
27. Cannon R.D., 1981 in "Optical Jets in Galaxies", ESA SP 162 p. 45
28. Carramiñana A., Chadwick P.M., Dipper N.A., et al., 1990 A&A 228, 327
29. Christiansen W.N., Frater R.H., Watkinson A., O'Sullivan J.D., Lockhart I.A., 1977 MNRAS 181, 183
30. Ciardullo R., Ford H.C., Williams R.E., Tamblyn P., Jacoby G.H., 1990 AJ 99, 1079
31. Clarke D.A., Burns J.O., Feigelson E.D., 1986 ApJL 300, L41
32. Clarke D.A., Burns J.O, Norman M.L., 1992 ApJ 395, 444
33. Combi J.A., Romero G.E., 1997 A&AS 121, 11
34. Condon J.J., Helou G., Sanders D.B., Soifer B.T., 1996 ApJS 103, 81
35. Cooper B.F.C., Price R.M., Cole D.J., 1965 Aust. J. Phys. 18, 589
36. Côté S., 1995, Ph. D. Thesis Mt. Stromlo and Siding Spring Observatories, Australian National University
37. Côté S., Freeman K.C., Carignan C., Quinn P.J., 1997 AJ 114, 1313
38. Cristiani S., Cappellaro E., Turatto M., et al. 1992 A&A 259, 63
39. Cunningham C.T., Ade P.A.R., Robson E.I., Radostitz J.V., 1984 MNRAS 211, 543
40. Danziger I.J., 1981 in "Optical Jets in Galaxies", ESA SP 162, p. 143
41. Davies R.L., Efstathiou G., Fall M., Illingworth G., Schecter P.L., 1983 ApJ 266, 41
42. de Vaucouleurs G., 1975, in *Stars and Stellar Systems*, Vol. 9, *Galaxies and the Universe*, ed. A. Sandage, M. Sandage & J. Kristian (Chicago: Univ. Chicago Press), p. 557
43. de Vaucouleurs G., de Vaucouleurs A., Corwin H.G., 1976, *Second Reference Catalogue of Bright Galaxies*, (Austin: Univ. of Texas Press),(RC2)
44. de Vaucouleurs G., 1993 ApJ 415, 10
45. de Zeeuw P.T., Franx M., 1991 ARAA 29, 239
46. Dermer C.D., Schlickeiser R., 1993 ApJ 416, 458
47. Döbereiner S., Junkes N., Wagner S.J., et al. 1996 ApJL 470, L15
48. d'Odorico S., di Serego Alighieri S., Pettini M., et al., 1989 A&A 215, 21
49. Dottori H.A., Fourcade C.R., 1973 A&A 23, 405
50. Drinkwater M.J., Combes F., Wiklind T., 1996 A&A 312, 771
51. Dufour R.J., van den Bergh S., 1978 ApJL 226, L73
52. Dufour R.J., van den Bergh S., Harvel C.A., et al. 1979 AJ 84, 284

53. Ebneter K., Balick B., 1983 PASP 95, 675
54. Eckart A., Cameron M., Rothermel H., et al., 1990a ApJ 363, 451
55. Eckart A., Cameron M., Genzel R., et al., 1990b ApJ 365, 522
56. Elvius A., Hall J.S., 1964 Bull. Lowell Obs. VI, 123
57. Evans R., 1986 IAU Circular no. 4208
58. Fanaroff B.L., Riley J.M., 1974 MNRAS 167, 31P
59. Feigelson E.D., Schreier E.J., Delvaille J.P., et al., 1981 ApJ 251, 31
60. Fichtel C.E., Bertsch D.L., Chiang J., et al. 1994 ApJS 94, 551
61. Fogarty W.G., Schuch N.J., 1975 Nature 254, 124
62. Frogel J.A., 1984 ApJ 278, 119
63. Frogel J.A., Gregory B., Kawara K., et al., 1987 ApJL 315, L129
64. Gardner F.F., Whiteoak J.B., 1976a MNRAS 175, 9P
65. Gardner F.F., Whiteoak J.B., 1976b Proc. A.S.A. 3, 63
66. Gardner F.F., Whiteoak J.B., 1979 MNRAS 189, 51P
67. Gehrels N., Cline T.L., Teegarden B.J., et al. 1984 ApJ 278, 112
68. Giles A.B., 1986 MNRAS 218, 615
69. Gopal-Krishna, Saripalli L., 1984 A&A 141, 61
70. Gouveia dal Pino E.M., Opher R., 1989 ApJ 342, 686
71. Graham J.A., 1979 ApJ 232, 60
72. Graham J.A., 1981 PASP 93, 291
73. Graham J.A., 1983 ApJ 269, 440
74. Graham J.A., Phillips M.M., 1980 ApJL 239, L97
75. Graham J.A., Price R.M., 1981 ApJ 247, 813
76. Grasdalen G.L., Joyce R.R., 1976 ApJ 208, 317
77. Griffin R.E., 1963 AJ 68, 421
78. Grindlay J.E., 1975 ApJ 199, 49
79. Grindlay J.E., Helmken H.F., Hanbury Brown R., Davis J., Allen L.R., 1975 ApJL 197, L9
80. Haddock F.T., Mayer C.H., Sloanaker R.M., 1954 ApJ 119, 456
81. Harding P., Jones T.J., Rodgers A.W., 1981 ApJ 251, 530
82. Harris G.L.H., Hesser J.E., Harris H.C., Curry P.J., 1984a ApJ 287, 175
83. Harris H.C., Harris G.L.H., Hesser J.E., McGillivray H.T., 1984b ApJ 287, 185
84. Harris H.C., Harris G.L.H., Hesser J.E., 1986 in *the Harlow Shapley Symposium on on Globular Cluster Systems in Galaxies*, IAU Symp. 126, eds. J.E. Grindlay & A.G.D. Phillips (Dordrecht: Reidel), p. 205
85. Harris G.L.H., Geisler D., Harris H.C., Hesser J.E., 1992 AJ 104, 613
86. Haslam C.G.T., Klein U., Salter C.J., et al. 1981, A&A 100, 209
87. Hawarden T.G., Elson R.A.W., Longmore A.J., Tritton S.B., Corwin H.G., 1981 MNRAS 196, 747
88. Hawarden T.G., Sandell G., Matthews H.E., Friberg P., Watt G.D., Smith P.A., 1993 MNRAS 260, 844
89. Haynes R.F., Cannon R.D., Ekers R.D., 1983 Proc. ASA 5, 241
90. Heckman T.M., Illingworth G.D., Miley G.K., van Breugel W.J.M., 1985 ApJ 299, 41
91. Hernquist L., Quinn P.J., 1988 ApJ 331, 682
92. Hernquist L., Quinn P.J., 1989 ApJ 342, 1
93. Herschel J.F.W., 1847, *Results of Astronomical Observations at the Cape of Good Hope* (London: Smith, Elder), pages 105 and 20 respectively
94. Hesser J.E., Harris H.C., van den Bergh S., Harris G.L.H. 1984 ApJ 276, 491
95. Hesser J.E., Harris H.C., Harris G.L.H., 1996 ApJL 303, L51
96. Hough J.H., Bailey J.A., Rouse M.F., Whittet D.C.B., 1987 MNRAS 227, 1P
97. Hubble, E., 1922 ApJ 56, 162
98. Hui X., Ford H.C., Ciardullo R., Jacoby G.H., 1993a ApJ 414, 463
99. Hui X., Ford H.C., Ciardullo R., Jacoby G.H., 1993b ApJS 88, 423
100. Hui X., Ford H.C., Freeman K.C., Dopita M.A., 1995 ApJ 449, 592
101. Hunter D.A., Gallagher J., Rice W.L., Gillett F.C., 1989 ApJ 336, 152
102. Hodge P.W., Kennicutt R.C., 1983 AJ 88, 296
103. Israel F.P., 1992 A&A 265, 487
104. Israel F.P., van Dishoeck E.F., Baas F., et al. 1990 A&A 227, 342
105. Israel F.P., van Dishoeck E.F., Baas F., de Graauw T., Phillips T.G., 1991 A&A 245, L13
106. Israel F.P., van der Werf P.P., Hawarden T.G., Aspin C., 1998 A&A submitted
107. Jablonka P., Bica E., Pelat D., Alloin D., 1996 A&A 307, 385
108. Jacoby G.H., Branch D., Ciardullo R., et al. 1992 PASP 104, 599
109. Jauncey D.L., Tingay S.J., Preston R.A., et al., 1995 Proc. Natl. Acad. Sci. USA 92, 11368
110. Joy M., Lester D.F., Harvey P.M., Ellis H.B., 1988 ApJ 326, 662
111. Joy M., Harvey P.M., Tollestrup E.V., et al., 1991 ApJ 366, 82

112. Jones P.A., McAdam W.B., Reynolds J.E. 1994 MNRAS 268, 602
113. Jones D.L., Tingay S.J., Murphy D.W., et al., 1996 ApJL 466, L63
114. Jones D.L., Wehrle A.E., 1997 ApJ 484, 186
115. Jourdain E., Bassani L., Roques J.-P., 1993 ApJ 412, 586
116. Junkes N., Haynes R.F., Harnett J.I., Jauncey D.L., 1993 A&A 269, 29
117. Kellerman, K.I., 1974 ApJL 194, L135
118. Kellerman K.I., Zensus J.A., Cohen M.H., 1997 ApJL 475, L93
119. Kinzer R.L., Johnson W.N., Dermer C.D., et al., 1995 ApJ 449, 105
120. Koornneef J., Israel F.P., 1996 New Astr. 1, 271
121. Kormendy J., Djorgovski S., 1989 ARAA 27, 235
122. Krolik J.H., Lepp S., 1989 ApJ 347, 179
123. Kunkel W.E., Bradt H.V., 1971 ApJL 170, L7
124. Lépine J.R.D., Braz M.A., Epchtein N., 1984 A&A 131, 72
125. Marcelin M., Boulesteix J., Courtès G., Milliard B., 1982 Nature 297, 38
126. Malin D.F., Quinn P.J., Graham, J.A., 1983 ApJL 272, L5
127. Marshall F.J., Clark G.W., 1981 ApJ 245, 840
128. Marston A.P., Dickens R.J., 1988 A&A 193, 27
129. Marston A.P., 1992 in *Relationships between Galactic Nuclei and Starburst Galaxies*, ASP Conference Series 31, p. 123
130. Mathieu A., Dejonghe H., Hui X., 1996 A&A 309, 30
131. Maiolino R., Rieke G.H., 1995 ApJ 454, 95
132. McElroy D.B., Humphreys R.M., 1982 PASP 94, 828
133. Meadows V., Allen D.A., 1992 Proc. A.S.A. 10, 104
134. Meier D.L., Jauncey D.L., Preston R.A., et al., 1989 AJ 98, 27
135. Miley G.K., 1980 ARAA 18, 165
136. Mills B.Y., 1952 Austral. J. Phys. 5, 266
137. Minniti D., Alonso M.V., Goudfrooij P., Jablonka P., Meylan G., 1996 ApJ 467, 221
138. Miyazaki S., Takahashi T., Gunji S., et al., 1996 PASJ 48, 801
139. Morganti R., Robinson A., Fosbury R.A.E., di Serego Alighieri S., Tadhunter C.N., Malin D.F., 1991 MNRAS 249, 91
140. Morganti R., Fosbury R.A.E., Hook R.N., Robinson A., Tsvetanov Z., 1992 MNRAS 256, 1P
141. Morini M., Anselmo F., Molteni D., 1989 ApJ 347, 750
142. Mouri H., 1994 ApJ 427, 777
143. Mushotzky R.F., Serlemitsos P.J., Becker R.H., Boldt E.A., Holt S.S., 1978 ApJ 220, 790
144. Newell E.B., Rodgers A.W., Searle L.T., 1969 ApJ 158, 699
145. Nicholson R.A., Bland-Hawthorn J., Taylor K., 1992 ApJ 387, 503
146. Norman M.L., Burns J.O, Sulkanen M.S. 1988 Nature 335, 146
147. O'Neill T., Tumer O.T., Zych A., White R.S., 1989 ApJ 339, 78
148. Osmer P.S., 1978 ApJL 226, L79
149. Packham C., Hough J.H., Young S., et al., 1996 MNRAS 278, 406
150. Paglione T.A.D., Jackson J.M., Ishizuki S., 1997 ApJ 484, 656
151. Paraskevoulos, J.S., 1935 Harvard Bulletin 890, 1
152. Perelmuter J.-M., 1995 ApJ 454, 762
153. Phillips M.M., 1993 ApJ 413, L105
154. Phillips M.M., Taylor K., Axon D.J., Atherton P.D., Hook R.N., 1984 Nature 310, 554
155. Phillips M.M., Phillips A.C., Heathcote S.R., 1987 PASP 99, 592
156. Phillips T.G., Ellison B.N., Keene J.B., et al. 1987 ApJL 322, L73
157. Preston R.A., Wehrle A.E., Morabito D.D., et al., 1983 ApJL 266, L93
158. Quillen A.C., de Zeeuw P.T., Phinney E.S., Phillips T.G., 1992 ApJ 391, 121
159. Quillen A.C., Graham J.R., Frogel J.A., 1993 ApJ 412, 550
160. Rice W., Lonsdale C.J., Soifer B.T. et al. 1988 ApJS 68, 91
161. Richter O.-G., Sackett P.D., Sparke L.S., 1994 AJ 107, 99
162. Riess A.G., Press W.H., Kirshner R.P., 1996 ApJ 473, 88
163. Rodgers A.W., Harding A.W., 1980, ApJL 236, L17
164. Romero G.E., Benaglia P., Combi J.A., 1997 A&AS 124, 307
165. Ruiz-Lapuente P., Lucy L.B., Danziger I.J., 1992 Mem. Soc. Astr. It. 63, 233
166. Rydbeck G., Wiklind T., Cameron M., et al. 1993 A&A 270, L13
167. Sadler E.M., Gerhard O.E., 1985 MNRAS 214, 177
168. Sandage A.R., Tammann G.A. 1974 ApJ 194, 559
169. Scarrott S.M., Foley N.B., Gledhill T.M., Wolstencroft R.D., 1996 MNRAS 282, 252
170. Schreier E.J., Feigelson E., Delvaille J., et al., 1979 ApJL 234, L39
171. Schreier E.J., Burns J.O, Feigelson E.D., 1981 ApJ 251, 523
172. Schreier E.J., Capetti A., Macchetto F., Sparks W.B., Ford H.J., 1996 ApJ 459, 535

173. Schiminovich D., van Gorkom J.H., van der Hulst J.M., Kasow S., 1994 ApJL 423, L101
174. Seaquist E.R., Bell M.B., 1986 ApJL 303, L67
175. Seaquist E.R., Bell M.B., 1990 ApJ 364, 94
176. Shain C.A., 1958 Aust. J. Phys 11, 517
177. Sheridan K.V., 1958 Aust. J. Phys. 11, 400
178. Shopbell P.L., Bland-Hawthorn J., Malin D.F., 1993 AJ 106, 1344
179. Simpson C., 1994 MNRAS 271, 247
180. Skibo J.G., Dermer C.D., Kinzer R.L., 1994, ApJL 426, L23
181. Slee O.B., Sheridan K.V., Dulk G.A., Little A.G., 1983 Proc. ASA 5, 247
182. Soria R., Mould J.R., Watson A.M., et al. 1996 ApJ 465, 79
183. Sparke L.S., 1982 ApJ 254, 456
184. Sparke L.S., 1996 ApJ 473, 810
185. Steinle H., Bennett K., Bloemen H., et al. 1998 A&A 330, 97
186. Storchi-Bergmann T., Bica E., Kinney A.L., Bonatto C., 1997 MNRAS 290, 231
187. Sugizaki M., Inoue H., Sonobe T., Takahashi T., Yamamoto Y., 1997 PASJ 49, 59
188. Sutherland R.S., Bicknell G.V., Dopita M.A., 1993 ApJ 414, 510
189. Tateyama C.E., Strauss F.M., 1992 MNRAS 256, 8
190. Telesco C.M., 1978 ApJ 226, L125
191. Terrell J., 1986 ApJ 300, 669
192. Thompson D.J., Bertsch D.L., Dingus B.L., et al., 1995 ApJS 101, 259
193. Tingay S.J., Jauncey D.L., Reynolds J.E., et al., 1998 ApJin press
194. Tonry J.L., Schecter P.L., 1990 AJ 100, 1794
195. Tonry J.L., 1991 ApJ 373, L1
196. Tornikoski M., Valtaoja E., Teräsranta H., et al. 1996 A&AS 116, 157
197. Tubbs A.D., 1980 ApJ 241, 969
198. Turner P.C., Forrest W.J., Pipher J.L., Shure M.A., 1992 ApJ 393, 648
199. Turner T.J., George I.M., Mushotzky R.F., Nandra K., 1997 ApJ 475, 118
200. Ubertini P., Bazzano A., Cocchi M., La Padula C., Sood R., 1993 A&AS 97, 105
201. van Albada T.S., Kotanyi C.G., Schwarzschild M., 1982 MNRAS 198, 303
202. van den Bergh S., 1976 ApJ 208, 673
203. van den Bergh S., Hesser J.E., Harris G.L.H., 1981 AJ 86, 24
204. van der Hulst J.M., Golisch W.F., Haschick A.D., 1983 ApJL 264, L37
205. van Dokkum P.G., Franx M., 1995 AJ 110, 2027
206. van Driel W., de Graauw Th., de Jong T., Wesselius P.R., 1993 A&AS 101, 207
207. van Gorkom J.H., Knapp G.R., Ekers R.D., et al., 1989 AJ 97, 708
208. van Gorkom J.H., van der Hulst J.M., Haschick A.D., Tubbs A.D., 1990 AJ 99, 1781
209. van Langevelde H.J., van Dishoeck E.F., Sevenster M.N., Israel F.P., 1995 ApJL 448, L123
210. Viegas S.M., Prieto M.A., 1992 MNRAS 258, 483
211. von Ballmoos P., Diehl R., Schoenfelder V., 1987 ApJ 312, 134
212. Wang B., Inoue H., Koyama K., et al. 1986 PASJ 38, 685
213. Webster B.L., Goss W.M., Hawarden T.G., Longmore A.J., Mebold U., 1979 MNRAS 186, 31
214. Weil M.L., Hernquist L., 1996 ApJ 460, 101
215. Whiteoak J.B., Gardner F.F., 1979, Proc. A.S.A. 3, 319
216. Whiteoak J.B., Gardner F.F., Höglund B., 1980, MNRAS 190, 17p
217. Wiklind T., Combes F., 1997 A&A 324, 51
218. Wild W., Eckart A., Wiklind T., 1997 A&A 322, 419
219. Wilkinson A., Sharples R.M., Fosbury A.E., Wallace P.T., 1986 MNRAS 218, 297
220. Quinn P.F., 1984 ApJ 279, 596
221. Zepf S.E., Ashman K.M., 1993 MNRAS 264, 611
222. Zickgraf F.-J., Humphreys R.M., Graham J.A., Phillips A., 1990 PASP 102, 920
223. Zirbel E.L., 1996 ApJ 473, 713